EXPLORATION OF TACTILE SPATIAL PERCEPTION

EXPLORATION OF A BAYESIAN MODEL OF TACTILE SPATIAL PERCEPTION

By SEYEDBEHRAD DEHNADI, BSc

A Thesis Submitted to the School of Graduate Studies in Partial Fulfillment of the Requirements for the Degree Master of Science

McMaster University

MASTER OF SCIENCE (2022)

Hamilton, Ontario, Canada (Neuroscience)

TITLE:	Exploration of a Bayesian Model of Tactile Spatial Perception
AUTHOR:	Seyedbehrad Dehnadi BSc (Neuroscience), McMaster University, Hamilton, Canada
SUPERVISOR:	Dr. Daniel Goldreich
NUMBER OF PAGES:	xii, 105

Abstract

The remarkable ability of the human brain to draw an accurate percept from imprecise sensory information is not well understood. Bayesian inference provides an optimal means for drawing perceptual conclusions from sensorineural activity. This approach has frequently been applied to visual and auditory studies but only rarely to studies of tactile perception. We explored whether a Bayesian observer model could replicate fundamental aspects of human tactile spatial perception. The model consisted of an encoder that simulated sensorineural responses with Poisson statistics followed by a decoder that interpreted the observed firing rates. We compared the performance of our Bayesian observer on a battery of tactile tasks to human participant data collected previously by our laboratory and others. The Bayesian observer replicated human performance trends on three spatial acuity tasks: classic two-point discrimination (C2PD), sequential two-point discrimination (S2PD), and two-point orientation discrimination (2POD). We confirmed the widely reported observation that C2PD is the least reliable method of assessing tactile acuity due presumably to the presence of non-spatial cues. Additionally, the Bayesian observer performed similarly to humans on raised letter and Braille character-recognition tasks. The Bayesian observer further replicated two illusions previously reported in humans: an adaptation-induced repulsion illusion and an orientation anisotropy illusion. Taken

together, these results suggest that human tactile spatial perception may arise from a Bayesian-like decoder that is unaware of the precise characteristics of its inputs.

Table of Contents

List of Figures

List of Tables

Notation, Definitions, and Abbreviations

List of Abbreviations

α	Adaptation
λ	Expected Spike Count
σ	Gaussian RF Sigma
2IFC	Two-interval Forced Choice
2PD	Two-point Discrimination Task
2POD	Two-point Orientation Discrimination Task
A	Tuning Curve Amplitude
AIRI	Adaptation Induced Repulsion Illusion
BCRT	Braille-character Recognition Task
C	Comparison
c	RF Center To Center Spacing
C2PD	Classic Two-point Discrimination Task
D	Data
d	Distance
I	Intensity
i	Index
J	Jitter Level
j	Model Index

k	Spike Count
L	Longitudinal
l	Hypothesis Index
M	Model
m	Magnitude Factor
O	1-point Stimulus
OAI	Orientation Anisotropy Illusion
P	Proximal
p	Position Of Point Stimulus
PSE	Point Of Subject Equality
R	Reference
r	Response Rate
RLRT	Raised-letter Recognition Task
s	Expected Stimulus-evoked Spike Count
S2PD	Sequential Two-point Discrimination Task
SA1	Slowly Adapting Type 1
SR	Stimulus Radius
T	Transverse
t	Time/duration
V	2-point Stimulus
x	Position Of RF Center
Y	Distal

Chapter 1

Introduction

1.1 Perception and Survival

The ability of humans to correctly estimate the state of the world amid uncertainty is crucial for our survival. For our ancestors, an error in judgment regarding a source of movement in bushes could have been fatal. Modern humans, if we make perceptual misjudgments, would face the same dire consequences each time we attempt to cross a street or walk down a staircase. Luckily, the human brain is adept at dealing with stimulus uncertainty. The brain's ability to infer the state of the external world is particularly impressive considering that nearly all input to the nervous system is subject to noise and, consequently, uncertainty. The mechanism by which the brain generates an accurate inference from imprecise sensory inputs is not well understood. Such inference requires the brain to distinguish signal from noise, but how is this accomplished?

1.1.1 What is Perception

We must first define what we mean by perception, and more specifically how it differs from sensation. Like many other conceptual terms denoting a mental process, while we may have an intuitive understanding of the term, it is exceedingly difficult to explicitly define it. Webster's dictionary defines perception as "awareness of the elements of environment through physical sensation". Although this is a good starting definition, it is incomplete as perception is far more than just the awareness of the environment. Perception also entails the process of interpreting, identifying, and categorizing elements in the environment. Sensation involves the acquisition of environmental signals through our senses. Perception involves the process by which we make sense of these signals.

1.2 Computational Models of Perception

1.2.1 Qualities of the model

The mechanism by which perception emerges from sensory information is a mystery. Empirical research such as neurophysiological and psychophysical studies has gotten us closer to uncovering this mechanism; however, the information obtained by these studies is often disconnected and segregated. We lack a unifying theory that explains how nervous systems encode, represent, and store sensory information, and how perception interprets this information. A promising complement to the empirical research is computational modelling, which aims to tackle the overarching encoding and decoding principles that may govern perception. Like piecing together a puzzle, a

good computational model has the power to contextualize empirical findings, summarize the multiplicity of findings, and uncover hidden truths. Different computational models are designed for a specific task and scope. In deciding which computational model to use to investigate human tactile spatial perception, we set two criteria. Our model needs to be Simplified/Idealized and Probabilistic.

Model Simplicity

Computational models can be largely categorized as descriptive, mechanistic, or interpretive (Dayan & Abbott, 2001). Descriptive models, as the name suggests, describe what neural circuits do by summarizing large amounts of experimental data compactly. Mechanistic models explain how the nervous system operates and propose neural mechanisms based on established circuitry and physiology. Lastly, interpretive models aim to understand what function the nervous systems are constructed to perform. These models explore the behavioural and cognitive significance and computational advantage of various aspects of nervous system operations. Depending on the research question, different levels of complexity and detail need to be employed in the model. A more detailed model does not necessarily make it superior (Dayan & Abbott, 2001). For a model to be effective, it needs to be detailed enough to answer the research question; more complexity can hinder the effectiveness of the model. Given the broad nature of our question, a mechanistic model would be too detailed for our work; thus, a descriptive model is more appropriate.

Probabilistic vs Deterministic Models

Characterizing the relationship between stimulus and response is difficult because neuronal responses are complex and variable. Neurons typically respond by producing complex spike sequences that reflect both the intrinsic dynamics of the neuron and the temporal characteristics of the stimulus. Neural responses can vary from trial to trial even when the same stimulus is presented repeatedly. This variable response pattern is due to a number of different potential sources, including variable levels of arousal and attention, and randomness associated with various biophysical processes that affect neuronal firing.

Deterministic models, as their name suggests, assume that the brain functions deterministically—for a given stimulus, the same response is elicited. These models are able to accurately predict the response pattern only if all their inputs are known. However, there remain many unknowns in regard to neural networks that make deterministic models inaccurate in practice. The complexity and trial-to-trial variability of action potential sequences make it unlikely that we can describe and predict the timing of each spike deterministically. Instead, we seek a model that can account for the probabilities of different evoked spike sequences. A probabilistic model assumes that perception reflects what is statistically likely to occur in reality, therefore mitigating the random effects of noise. A great deal of psychophysical and electrophysiological evidence suggests that given the same stimulus, the variable output is observed (Waschke et al., 2021). The source of this variability or noise is still in question, and whether the noise is a by-product of neurological processors or an intentional computational mechanism is still unknown.

Sensory Models

Bayesian inference provides an optimal method for drawing perceptual conclusions from sensorineural activity. Thus, the Bayesian framework provides a useful normative model with which to study perception. A growing number of studies in vision, hearing, and multi-modal perception have shown that human performance conforms closely to the predictions of Bayesian models (Geisler & Kersten, 2002; Ma et al., 2006; Stocker & Simoncelli, 2006). The near-optimal performance of humans has led many researchers to suspect that perception involves Bayesian-like calculations; however, the extent to which the brain uses Bayesian inference is unclear. Most previous studies have focused on non-tactile senses. In the present study, our goal is to investigate whether observed trends in tactile perception – particularly, passive tactile spatial perception – are consistent with the Bayesian framework.

1.3 Somatosensory Transduction Pathway

When an object touches the skin, mechanoreceptors encode the properties of the object as response patterns. These mechanoreceptors are distinguished based on their receptive field, their rates of adaptation and the type of stimulation to which they respond (Jones & Smith, 2014). Merkel cells, which are innervated by slowly adapting type 1 (SA1) afferents, detect static stress and sustained pressure (Maricich et al., 2009), making them ideal for encoding fine tactile spatial information. SA1 afferent inputs from the hands ascend via the dorsal columns to synapse in the cuneate nucleus of the medulla oblongata. The signal subsequently passes through the medial

lemniscus to the ventroposterolateral thalamus, and from there to the primary somatosensory cortex (Pei et al., 2009). The brain somehow decodes the evoked firing patterns to infer the properties of the felt object from the observed pattern of neural activity. This inference is presumably based on a series of assumptions the brain makes about the world.

1.4 Our Bayesian Model

Similar to the human transduction pathway, our simulations involve an encoding and a decoding stage. The encoding stage (forward-processing or generative stage) converts sensory stimuli into spatial patterns of action potentials characterized by Poisson firing rate variability—the mean firing rate is approximately equal to the variance of the firing rate—that are typical of the firing rates cortical sensory neurons (Moreno-Bote, 2014; Sripati et al., 2006). The decoding stage uses Bayesian inference to solve the inverse problem: inferring the stimulus structure from the observed spatial pattern of spike counts. The two ingredients considered by the Bayesian decoder are the likelihood function and the prior probability distribution. The likelihood function is the probability of the observed neural activity as a function of the tactile stimulus structure based on the internal representation of the generative stage. The prior probability distribution is the probability of occurrence of each tactile stimulus structure based on previous experiences or task instruction. The general formula for Bayesian inference is:

$$posterior \propto likelihood \times prior \tag{1.4.1}$$

The Bayesian inference approach has scarcely been applied in studies of tactile perception; therefore, it has been unclear whether the Bayesian brain model can extend successfully to all senses. We investigated whether the Bayesian framework is able to provide a unifying explanation of human performance on some of the most commonly used tactile spatial perception tasks involving punctate stimuli. We considered two categories of experiments—tactile acuity tasks and illusion tasks—to investigate the general applicability of our model.

1.5 Tasks Simulated

1.5.1 Tactile Spatial Acuity Tasks

Tactile spatial acuity can be assessed by different variations of two-point discrimination tasks (2PDs) and letter recognition tasks. The original variation of two-point discrimination task was introduced by E. H. Weber in 1834, in which, two spatially separated points contact the skin simultaneously, and participants are asked whether they felt one point or two (Helen et al., 2018). As the distance between the two points decreases, it becomes more difficult for the participants to distinguish between two points and one point. In practice, this classic two-point discrimination task (C2PD) suffers from highly variable within and between subjects' responses (Craig & Johnson, 2000; Johnson & Phillips, 1981a; Stevens & Patterson, 1995). Even though the two-interval forced choice (2IFC) variation of this task could mitigate some of these practical problems, it apparently still suffers from a fundamental problem—evident by above 50% performance at 0.0 mm stimulus separation distance (Johnson & Phillips, 1981b).

Several purportedly more rigorous alternative tasks have been suggested, such as the sequential two-point discrimination task (S2PD), in which participants are asked to judge whether two successive points of stimulation were applied in a proximal or a distal sequence (Mancini et al., 2014), and two-point orientation discrimination tasks (2POD), in which participants are asked to discriminate the orientation of two simultaneous points of contact (Tong et al., 2013). Using our Bayesian observer model, we investigated the possible causes for C2PD's shortcomings, and whether 2POD and S2PD are valid alternatives to C2PD.

Other methods to assess tactile spatial acuity include raised-character recognition tasks. We looked at two variations of this task, letter recognition (RLRT) and braille character recognition (BCRT). In this task, participants are asked to identify the letter stimulus presented to them (Johnson & Phillips, 1981b). We investigated whether our Bayesian observer could replicate the human participant confusion matrices on these tasks.

1.5.2 Illusion Tasks

Illusions are a powerful tool to reveal underlying perceptual mechanisms. Under the Bayesian framework, illusions can arise from sub-optimal decoders with either faulty likelihood function or prior probability distribution. A faulty likelihood function is due to a decoder's erroneous internal representation of the generative stage. Many visual illusions have already been explained by the Bayesian framework (Geisler & Kersten, 2002), and this approach has been less-frequently applied to the investigation of tactile illusions (Goldreich, 2007; Goldreich & Tong, 2013; Tong et al., 2016).

Similarly, we investigated whether tactile illusions such as adaptation induced repulsion illusion (AIRI) and orientation anisotropy illusion (OAI) could plausibly result from a Bayesian inference process. Inspired by visual aftereffect illusions (Schwartz et al., 2006), Li et al. (2017) discovered AIRI in which sensory adaptation causes the perceived location of a stimulus to shift away from the adapted area. Longo and Haggard (2011) discovered OAI in which the transverse distances on the dorsum of the hand are perceived larger than the same vertical distances. Unlike the acuity tasks in which we used an optimal decoder, to simulate illusion tasks, we created sub-optimal decoders. By manipulating assumptions that our sub-optimal decoder makes, we discovered situations in which these perceptual errors arise.

Chapter 2

Method

2.1 General Model

Our Bayesian model comprises of two computational stages, an encoding and decoding stage. The encoding stage simulates stimulus transduction, and the decoding stage simulates source inference. To make our model generalizable, we have adopted a dimensionless unit, c, to refer to the center-to-center spacing distance between RFs. All other length variables are expressed in terms of this unit. By inserting the appropriate value for c, we are able to scale our model for different body locations.

2.1.1 Encoder

The encoding stage simulates the spiking patterns of cortical neurons in response to tactile stimuli based on the response properties of modelled receptive fields (2.1A). The encoder model space is a 10c×10c patch of simulated skin that is innervated by a grid of N cortical neurons with 2D Gaussian function RF shapes (2.1B). The Gaussian

functions are defined by two parameters, standard deviation (σ) and amplitude (A). For all sensory tasks, we simulated individual participants with the same number of RFs and spacing but with a varying shift in the transverse phase to avoid idiosyncratic results (2.1C). RF positions are calculated as follows:

$$\begin{aligned} x_1 &\sim U(-\frac{1}{2}, \frac{1}{2}) \cdot c \\ x_{i+1} &= x_i + c \end{aligned} \tag{2.1.1}$$

where x is position of RF center and c is RF center to center spacing. The position of the first RF center is jittered by half of RF spacing.

For testing the effect of jittering the individual neuron RF properties—such as jittering amplitude, sigma, and spacing—within a given participant on performance, we used a similar formula:

$$\begin{aligned} A_i &= A \cdot e^X \\ \sigma_i &= \sigma \cdot e^X \\ x_{i+1} &= x_i + c \cdot e^X \\ X &\sim U(\ln \frac{1}{J}, \ln J) \end{aligned} \tag{2.1.2}$$

where A is tuning curve amplitude, σ is gaussian RF sigma, c is RF center to center spacing, J is the jitter level, X is a double-precision floating-point numeric number sampled from a uniform distribution defined by $U(\ln \frac{1}{J}, \ln J)$.

A point stimulus was defined by its position (p_x, p_y) on the skin patch. For a given point stimulus, the encoder calculates the expected stimulus-evoked spike count, s_i,

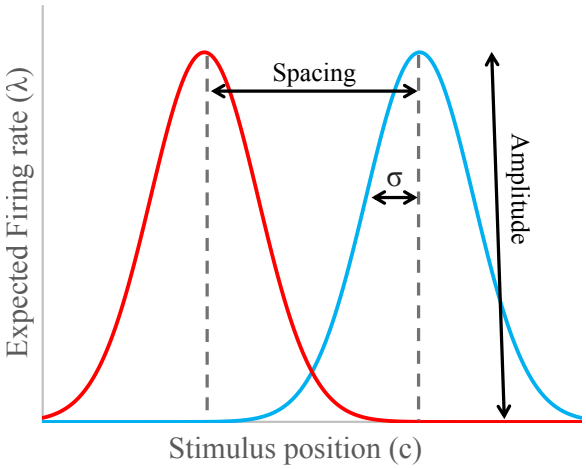

(A) RF Characteristics

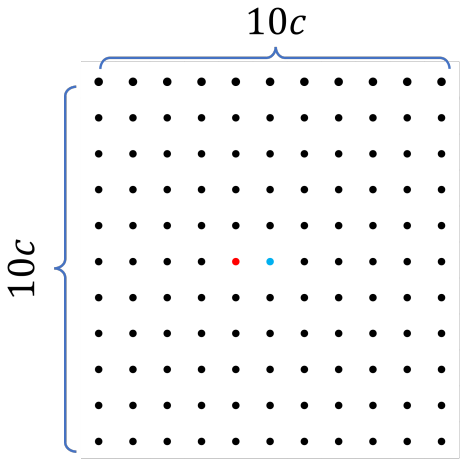

(B) Skin Space

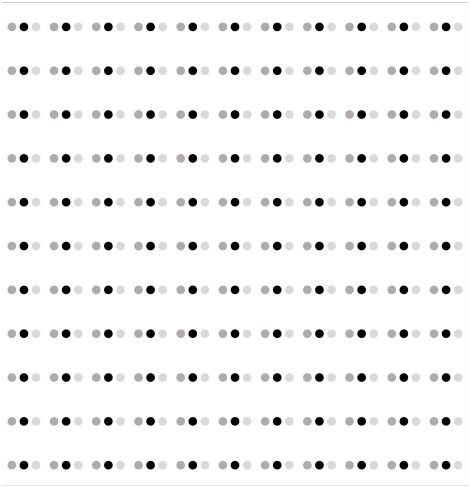

(C) RF Position Transverse Phase Shift

Figure 2.1: The model skin patch. **(A)** The model skin patch is represented by a square array of dots, in which each dot corresponds to a neuron's RF center. **(B)** Each neuron is characterized by its amplitude (A), sigma (σ) and their spacing to nearby RF centers (c). Depending on the task the sigma and spacing is scaled to match the location of the task on the body. **(C)** Three set of RF centers shown each corresponding to three different participants.

of a neuron based on the Gaussian function of distance from the neuron's RF center:

$$s_i = I \times Ae^{-\frac{d_i^2}{2\sigma^2}}, d_i = \sqrt{((p_y - y_i)^2 + (p_x - x_i)^2)} \tag{2.1.3}$$

where I is stimulus intensity, A is the Tuning curve amplitude, x_i and y_i denote the coordinate of the RF centers, and p_x and p_y denote stimulus coordinate. Values used in the simulation for these variables can be found in the Appendix.

Stimulus intensity (I) represents the skin indentation depth of a point stimulus. In order to investigate practical aspects of human experimentation, we simulated the use of two different control paradigms; displacement control and force control. In the displacement control paradigm, the stimulus intensity for each point is the same; in the force control paradigm, the stimulus intensity for each point is inversely proportional to the number of points for that task. We calculated the tuning curve amplitude based on the spike data collected previously from extracellular recordings of neurons in cortical area 3b of macaque monkeys in response to a punctate stimulus (Pei et al., 2009), as shown here,

$$A = r_{ON} \times t_{ON} + r_{SUSTAIN} \times t_{SUSTAIN} + r_{OFF} \times t_{OFF} \tag{2.1.4}$$

where r_{ON}, $r_{SUSTAIN}$,and r_{OFF} are the ON, SUSTAIN, and OFF response rate respectively, and t_{ON}, $t_{SUSTAIN}$, and t_{OFF} are ON, SUSTAIN, and OFF response time respectively.

We assumed linear summation of expected stimulus-evoked spike count to multi-point stimuli. Our model considers two separate sources of noise, spontaneous cortical activity and independent Poisson neural variability (Vazquez et al., 2013). A

stimulus-evoked spike count, k_i, for each neuron is randomly sampled from a Poisson distribution with a mean expected spike count, λ_i, such that:

$$\lambda_i = s_i + r_{spontaneous} \times t_{total}, k_i \sim Poisson(\lambda_i) \tag{2.1.5}$$

where $r_{spontaneous}$ is the spontaneous firing rate and t_{total} is the total stimulus duration.

The spike counts from each cortical neuron are then sent to the decoder for processing. For 2IFC experiments, there are two intervals of data creation. The spike count data resulting from the first interval (D_1) and the second interval (D_2) are sent to the decoder.

2.1.2 Decoder

The decoder processes the spike count data, D, to provide probabilistic estimates of stimulus features. To do so, the decoder considers a range of hypotheses for stimulus features (i.e., stimulus location). We assumed that the decoder has an internal representation of the generative model; meaning, the decoder was aware of the encoding stage RF characteristics (i.e., the Gaussian function, spacing, sigma, amplitude and positions), expected spike count, linear summation of spike count, spontaneous noise, and Poisson-like firing variability. For each hypothesis, H_l, the decoder calculates the expected spike count for all the neurons (λ) according to the equation 2.1.5. The decoder then uses λ to calculate the likelihood, $P(D \mid H_l)$:

$$P(D \mid H_l) = \prod_i \frac{e^{-\lambda_i} \times \lambda_i^{k_i}}{k_i!} \tag{2.1.6}$$

where l is hypothesis index, i is neuron index; there are 121 neurons in total.

To avoid numeric underflow when calculating the likelihoods, we calculated the log-likelihoods, found the maximum log-likelihood, subtracted the maximum log-likelihood from log-likelihoods, summed all the log-likelihoods, and exponentiated the log-likelihoods. This method is the same as multiplying likelihoods by a normalizing constant. This procedure does not affect the posterior PDF because the posterior PDF is only affected by the relative likelihoods of the hypotheses.

$$P(D \mid H_l) = e^{\ln(\prod_i \frac{e^{-\lambda_i} \times \lambda_i^{k_i}}{k_i!})} = e^{\sum_i k_i \ln(\lambda_i) - \lambda_i - \ln(k_i!)} \tag{2.1.7}$$

$$\frac{1}{e^{ML}} \times P(D \mid H_l) = e^{\sum_i k_i \ln(\lambda_i) - \lambda_i - \ln(k_i!) - ML} \tag{2.1.8}$$

where ML is the maximum log-likelihood.

For 2IFC tasks, the decoder needs to consider composite hypotheses, M_j, with their own range of sub-hypotheses regarding stimulus feature. We assume a uniform prior over these sub-hypotheses; therefore, the priors are reciprocal of the number of sub-hypotheses in each composite hypothesis. For a given M_j, the decoder calculates the composite hypothesis likelihood as marginal likelihood:

$$P(D \mid M_j) = \sum_l P(D \mid H_l, M_j) P(H_l \mid M_j) \tag{2.1.9}$$

where D is the data the decoder receive, and H_l is a sub-hypothesis.

For 2IFC tasks, the decoder considers two composite hypotheses, M_1 and M_2, corresponding to different stimulus presentations. Based on equation 2.2.7, the decoder calculates the posterior probability of these hypotheses using the calculated

composite hypothesis likelihoods:

$$P(M_j \mid D_i, D_2) = \frac{P(D_1, D_2 \mid M_i)P(M_i)}{P(D_1, D_2 \mid M_1)P(M_1) + P(D_1, D_2 \mid M_2)P(M_2)} \tag{2.1.10}$$

where D_1 and D_2 are data from the first and second interval respectively.

When the posterior odds $\frac{P(M_1 \mid D_1, D_2)}{P(M_2 \mid D_1, D_2}$) is greater than one, the decoder reports M_1 as trial response, otherwise M_2 is reported as the trial response. To make sure that all stimuli are detected by the decoder, we considered a composite hypothesis, M_3, that the spike counts are due to spontaneous noise. We then took the average posterior probability of M_3 over all trials. For the default experimental procedure, we confirmed that M_3 was less than 0.05.

2.2 Spatial Acuity Tasks

The two-point discrimination tasks were simulated using 2IFC paradigm in which each trial consisted of two possible stimulus sequences (2.2). The decoder has to make a judgement regarding which stimulus sequence was presented. For this purpose, the decoder considers a composite hypothesis for each of the two possible stimulus sequences. The decoder subsequently calculates the Bayes factor and reports its answer.

C2PD

The two composite hypotheses that the decoder considers are M_{VO} and M_{OV}. M_{VO} corresponds to D_1 being the result of two-point stimulus, and D_2 being the result of

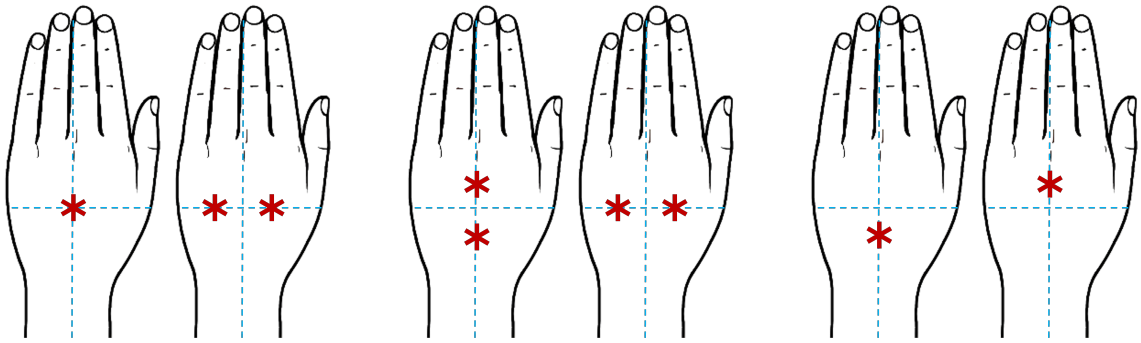

(A) C2PD **(B)** 2POD **(C)** S2PD

Figure 2.2: Schematic of two-point discrimination tasks. The asterisks are the stimulus location. All points are centered at the center of the skin patch. In C2PD, a point is given at one interval, and two points of varying separation is given at the other interval **(A)**. In 2POD, two-point stimulus of varying separation is given longitudinally at one interval and transversally at the other **(B)**. In S2PD, a point is given at the proximal location at one interval and the distal location at the other; such that both points are equidistant from the center point **(C)**.

one-point stimulus. M_{OV} corresponds to the alternative stimulus presentation order. To find the likelihood of each composite hypothesis, the decoder finds the marginal likelihoods as follows:

$$P(D_1, D_2 \mid M_{OV}) = \sum_d P(D_1 \mid H_O) P(D_2 \mid H_{V_d}) P(H_d \mid M_{OV}) \tag{2.2.1}$$

$$P(D_1, D_2 \mid M_{VO}) = \sum_d P(D_1 \mid H_{V_d}) P(D_2 \mid H_O) P(H_d \mid M_{VO}) \tag{2.2.2}$$

To find the probability that at any given interval the data are due to a two-point stimulus $P(D \mid H_{V_d})$, the decoder hypothesizes possible pairs of points that

are separated from each other at distances (d) of $0c$ to $4c$ at $\frac{2}{15}c$ steps. To find the probability that any given interval, the data are due to a one-point stimulus $P(D \mid H_O)$, the decoder considers a stimulus at the center of the skin patch.

2POD

The two composite hypotheses that the decoder considers are M_{TL} and M_{LT}. M_{TL} corresponds to D_1 being the result of transverse stimulus and D_2 being the result of a longitudinal orientated stimulus pair. M_{LT} corresponds to the alternative stimulus presentation. To find the likelihood of each composite hypothesis, the decoder finds the marginal likelihood:

$$P(D_1, D_2 \mid M_{TL}) = \sum_d P(D_1 \mid H_{T_d}) P(D_2 \mid H_{L_d}) P(H_d \mid M_{TL}) \tag{2.2.3}$$

$$P(D_1, D_2 \mid M_{LT}) = \sum_d P(D_1 \mid H_{L_d}) P(D_2 \mid H_{T_d}) P(H_d \mid M_{LT}) \tag{2.2.4}$$

To find the probability that at any given interval the data are due to a transverse stimulus $P(D \mid H_{T_d})$, the decoder hypothesizes possible pairs of points in the transverse direction that are separated at distances (d) of $0c$ to $4c$ at $\frac{2}{15}c$ steps. Similarly, to find the $P(D \mid H_{L_d})$, the decoder hypothesizes possible pairs of points but in the longitudinal direction.

S2PD

The two composite hypotheses that the decoder considers are M_{YP} and M_{PY}. M_{YP} corresponds to D_1 being the result of distal stimulus and D_2 being the result of the proximal stimulus. M_{PY} corresponds to the alternative stimulus presentation. To find the likelihood of each composite hypothesis, the decoder finds the marginal likelihood:

$$P(D_1, D_2 \mid M_{YP}) = \sum_d P(D_1 \mid H_{Y_d}) P(D_2 \mid H_{P_d}) P(H_d \mid M_{YP}) \tag{2.2.5}$$

$$P(D_1, D_2 \mid M_{PY}) = \sum_d P(D_1 \mid H_{P_d}) P(D_2 \mid H_{Y_d}) P(H_d \mid M_{PY}) \tag{2.2.6}$$

To find the probability that at any given interval the data are due to proximal stimulus $P(D \mid H_Y)$, the decoder hypothesizes x positions that are away from the transverse-line at distances (d) of $0c$ to $2c$ at $\frac{1}{15}c$ steps. To find $P(D \mid H_P)$, the decoder hypothesizes x positions that are away from the transverse-line at distances (d) of $0c$ to $-2c$ at $-\frac{1}{15}c$ steps.

2.2.1 Threshold

To summarize the Bayesian observer's performance in the 2PD tasks, we used the 76% threshold as the metric. The 76%-correct threshold is the stimulus value at which the Bayesian observer's proportion of correct response is 76%. For a 2IFC task, the 76% threshold is equivalent to the stimulus value at which $d' = 1$ (Colman, 2009).

To find the 76% threshold of our psychometric functions we used linear interpolation. For tasks that involved a large number of simulations, we used a Bayesian adaptive method (Kontsevich & Tyler, 1999) to find the threshold.

2.2.2 Letter Recognition Task

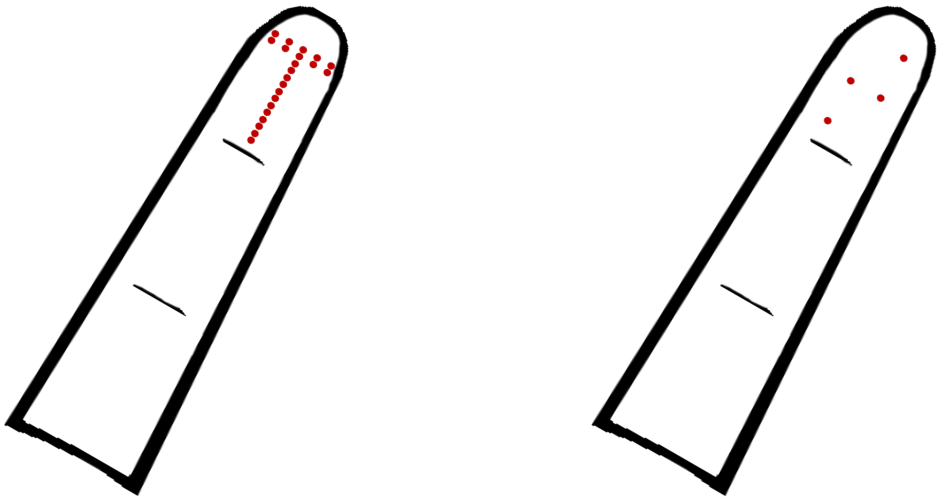

(A) Raised Letter **(B)** Braille Letter

Figure 2.3: Letter Recognition Task Schematic. Example of a raised letter and a Braille character stimulus on a fingertip. **(A)** The raised letter T stimulus consists of 22 points in which the transverse distance between points is twice as long as the longitudinal distance, modelled after optacon letter presentation (Craig, 1976). **(B)** The Braille character representation of the letter T consists of four points with equal distance to their neighbouring point. For both tasks, the participants need to identify the stimulus letter given to them.

Both braille and raised letter recognition tasks follow a similar encoding and decoding process (2.3). In the encoding stage, the letters are converted to a series of

points. Each dot in a Braille character is considered as one point (i.e. the braille character representing the letter Z, ⠵, consists of four points). The Braille characters' dimensions were modeled after Loomis (1982). For the raised letter recognition task, we converted uppercase English alphabet letters with Microsoft Sans Serif font to a 4-bit image data and subsequently to a bitmap. Each pixel in the bitmap represented a specific point, the position of which was calculated such that the overall height of the letters matched the height of the letters used by Craig (1979). We adjusted the font size such that the number of points for each letter roughly matched the number of points produced by the Optacon in Craig (1979). Under the force-control paradigm, we normalized the stimulus intensity of each point such that the sum of stimulus intensities of all the points within a letter was equal across letters. For each letter/character presented, the decoder considered twenty-six possible letter hypotheses. Based on Bayes' theorem, the decoder can calculate the posterior probability of each hypothesis as:

$$p(H_l \mid D) = \frac{P(D \mid H_l)P(H_l)}{\sum_j P(D \mid H_j)P(H_j)} \tag{2.2.7}$$

The hypothesis with the highest posterior probability was reported as the trial response. The results were then summarized in a form of a confusion matrix. We simulated our letter recognition tasks based on the data gathered from Craig (1979) and Loomis (1982). To fit our simulated model to human participants' data, we used a gradient descent algorithm to adjust the stimulus intensity as a free parameter such that the average proportion correct in the confusion matrix diagonal (hit rate) matched the human confusion matrix. We investigated the top twenty most confusing letter pairs based on the off-diagonal highest response letter pairs. The Pearson

correlation of simulated and human confusion matrices was taken.

We also explored the effect of stimulation mode on model performance. We looked at three different modes of stimuli presentation, the static mode, the repeated static mode, and the movement mode. In both the static mode and the repeated static mode, the letters are presented at the center of the skin patch. However, in the repeated static mode, the letters are presented multiple times at the same location (same position multiple sampling). In the movement mode, to simulate the movement of letters on the skin, the letters are presented along the skin over the distance of one RF center to center spacing length following this formula:

$$\Delta x = \frac{c \times i}{step\,count} - \frac{c}{2} \tag{2.2.8}$$

where step count represents the number of stimulus steps.

2.3 Illusion Tasks

2.3.1 Adaptation Induced Repulsion Illusion (AIRI)

In this experiment, the participants are presented with a two-point stimulus on both the comparison and the reference arm (2.4). The stimulus separation distance in the reference arm is held constant, while the separation distance in the comparison arm is varied. Participants are asked whether the separation distance was greater on the comparison or the reference arm. Under the adaptation paradigm, the center of the reference arm is adapted. Li et al. (2017) hypothesized that the adaptation-induced repulsion illusion could be explained by a Bayesian decoder that is unaware of the adaptation states of its neurons. To simulate adaptation, we used an adapting

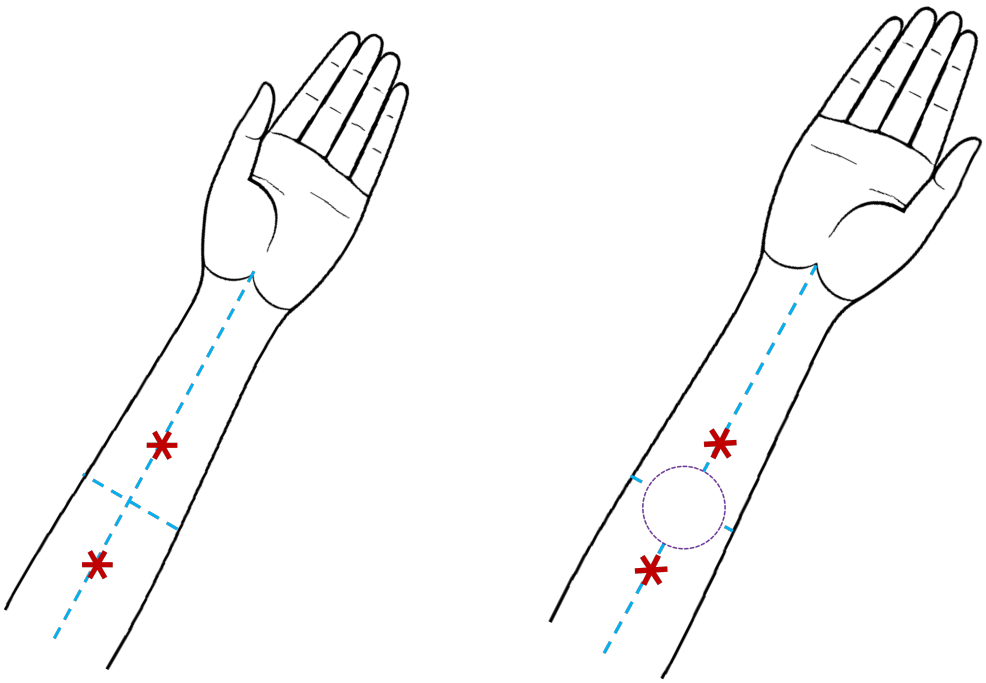

(A) Comparison Arm

(B) Reference Arm

Figure 2.4: Adaptation Induced Repulsion Illusion Schematic. Illustration of comparison **(A)** and the reference arm **(B)** in the AIRI. The asterisks are the stimulus location. The dashed circle represents the area of adapting stimulus at the center of the skin patch. The stimulus separation in the reference arm stays constant, but the separation distance of the stimulus in the comparison arm varies.

stimulus at the center of the skin patch which attenuates the response of the cortical neurons depending on their position relative to the adapting stimulus. Neurons with RFs that fall under the area of the adapting stimulus are uniformly adapted using the following equation:

$$s_{i,adapted} = s_{i,unadapted}(1 - \alpha) \tag{2.3.1}$$

where α ranges from 0 to 1, with 0 meaning completely unadapted, and 1 meaning completely adapted.

Neurons with RF centers that fall outside of the area of adapting stimulus are adapted using the following equation:

$$s_{i,adapted} = s_{i,unadapted}(1 - e^{-\frac{(d_i - r)^2}{2\sigma^2}} \cdot \alpha) \tag{2.3.2}$$

where r is the radius of adapting stimulus and d_i is the distance of RF centers to the center of adapting stimulus.

The decoder considers two composite hypotheses, $M_{C>R}$ and $M_{R>C}$. $M_{C>R}$ consists of sub-hypotheses that the comparison stimulus separation distance is greater than the reference stimulus separation distance, and $M_{R>C}$ consists of sub-hypotheses that the reference stimulus separation distance is greater than the comparison stimulus separation distance.

To test whether adaptation awareness affects the decoder's response, we made the decoder's internal representation of the generative stage unadapted (α=0). As a control, we also simulated the task with no adaptation.

2.3.2 Orientation Anisotropy Illusion (OAI)

On each trial, two pairs of stimuli were applied sequentially to the hand, one pair oriented longitudinally and the other pair oriented transversely (2.5). Both pairs of stimuli shared a common center. The separation distance along the longitudinal axis was held constant but the separation distance along the transverse axis was varied. Participants judged which separation distance felt larger. To make this judgement, our decoder considers two composite hypotheses, $M_{L>T}$ and $M_{T>L}$. $M_{L>T}$ corresponds to the composite hypothesis that the separation distance in the longitudinal axis is greater than the separation distance in the transverse axis, and$M_{T>L}$ corresponds to transverse separation distance being larger than the longitudinal. To find the probability of $M_{L>T}$, the decoder considers all the possible pairs of hypotheses in which the longitudinal distance (d_L) is greater than the transverse distances (d_T). The decoder is able to find the model likelihoods using the equation:

$$P(D_1, D_2 \mid M_{L>T}) = \sum_{d_L=\frac{4c}{15}}^{4c} P(D_1 \mid H_{d_L}) P(H_{d_L}) \sum_{d_T=0}^{d_L-\frac{2c}{15}} P(D_2 \mid H_{d_T}) P(H_{d_T}) \quad (2.3.3)$$

$$P(D_1, D_2 \mid M_{T>L}) = \sum_{d_T=\frac{4c}{15}}^{4c} P(D_1 \mid H_{d_T}) P(H_{d_T}) \sum_{d_L=0}^{d_T-\frac{2c}{15}} P(D_2 \mid H_{d_L}) P(H_{d_L}) \quad (2.3.4)$$

Unlike our other simulations, we made the RF geometry and center-to-center

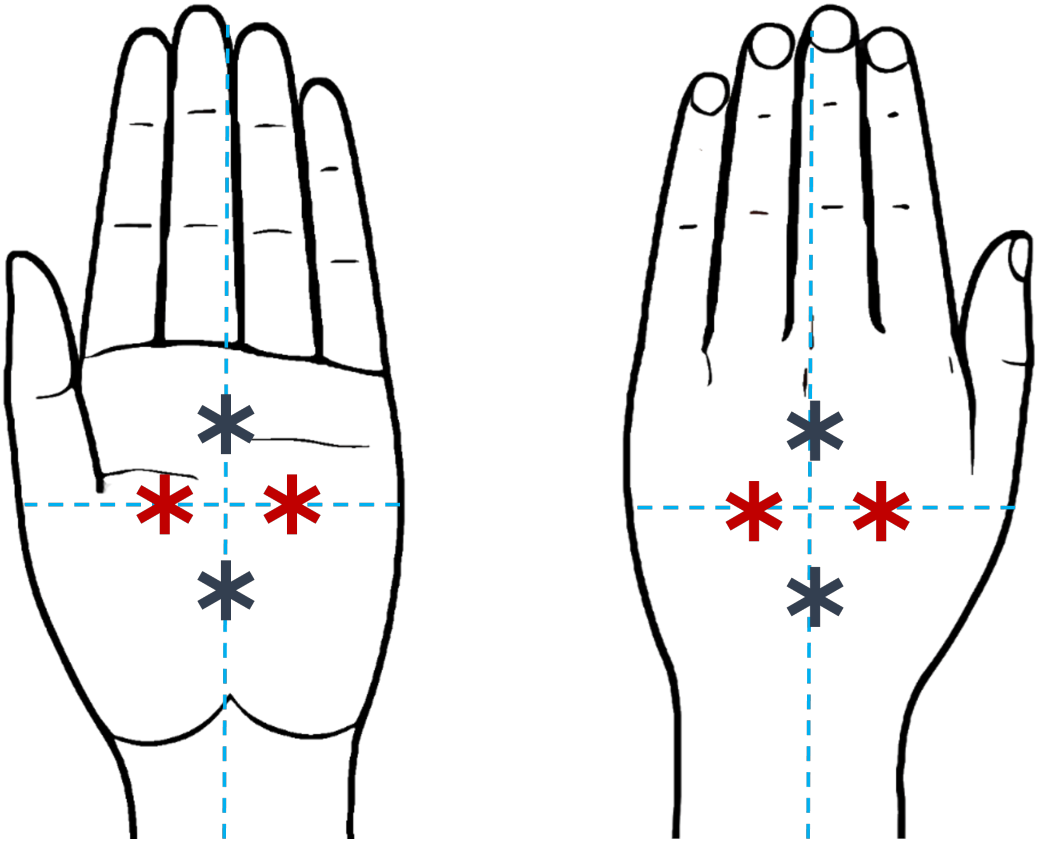

(A) Palm **(B)** Dorsum

Figure 2.5: Orientation Anisotropy Illusion Schematic. Illustration of palm **(A)** and dorsum **(B)** of the hand in OAI. The asterisks denote stimulus locations. The stimulus separation distance along the longitudinal axis was held constant, and the stimulus separation distance along the transverse axis varied. For a given hand, the participants are asked to judge whether the stimulus separation distance in the transverse direction was greater than the stimulus direction in the longitudinal direction.

spacing anisotropic. This was necessary to consider due to the reported RF shape differences and mapping in the dorsum and the palm of the hand. A cortical mapping study with owl monkeys (Merzenich et al., 1987) suggests that on average the RFs on the dorsum of the hand are more vertically elongated and spaced closer horizontally than the ones on the palm of the hand.

Chapter 3

Two Point Discrimination Results

3.1 Force-Control vs Displacement-Control

The mean performance of 2POD, C2PD, and S2PD is show in figure 3.1. To compare the performance of these tasks, we simulated two testing paradigms, force-control and displacement-control. In the force-control paradigm, the intensity of a point stimulus was adjusted such that the total intensity, the summation of all stimulus point intensities in a given interval, remained constant across stimulus intervals and tasks. Under the force-control paradigm, the point-stimulus intensity of S2PD was set to 1.0, the point-stimulus intensity of 2POD was set to 0.5, and the point-stimulus intensity of C2PD was set to 0.5 for the 2-point intervals and to 1.0 for the in 1-point intervals. Under this paradigm, the total spike count, on average, in a given trial is the same across tasks. In the displacement-control paradigm, the intensity of a point stimulus remains constant across tasks.

Under the displacement-control paradigm, the point-stimulus intensity of S2PD, 2POD, and C2PD tasks was set to 1.0. As shown in Fig. 3.1A, under force-control,

S2PD performance was higher than 2POD followed by C2PD. However, under displacement control, C2PD outperformed the other two 2PD tasks (Fig. 3.1B). The performance of S2PD remained the same because the 1-point stimulus intensity did not differ under the two paradigms; however, the performance of 2POD increased as the 2-point stimulus intensity was greater under the displacement-control paradigm. Under the displacement-control paradigm, the total stimulus intensity of the 2-point interval is greater than that of the 1-point interval. This means that the Bayesian observer receives more spike counts on average in the 2-point intervals than in the 1-point intervals. Because C2PD has both 2-point stimulus and 1-point stimulus intervals, the Bayesian observer can distinguish two points from one point based on total number of spikes in the neuronal population, even when the two points cannot be individually perceived (magnitude cue). The discrepancy in the total interval spike count in C2PD results in markedly higher performance under the displacement-control paradigm, evident by close to 100% performance at all separation distances (Fig. 3.1B). Because both 2POD and S2PD use the same number of stimulus point(s) across their intervals, their performance does not benefit from the magnitude cue.

3.2 Magnitude Factor

The mathematical representation of the magnitude cue, the magnitude Factor (m), is:

$$m = \frac{I_V}{I_O} \tag{3.2.1}$$

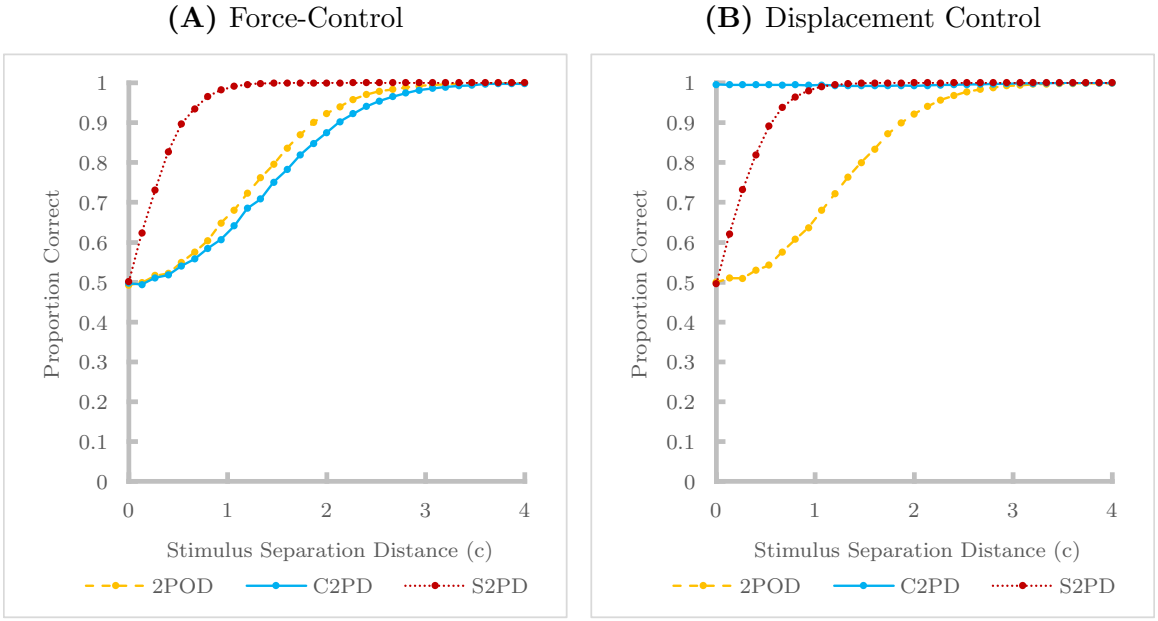

Figure 3.1: Two Point Discrimination Tasks Performance Comparison. Bayesian observer's proportion correct versus stimuli separation distance for 2POD, C2PD, and S2PD under force-control **(A)** and displacement control **(B)**.

where I_V is the stimulus intesity of a point in the 2-point interval and I_O is the 1-point interval stimulus intensity.

In the force-control version of C2PD, m=0.5, and in the displacement-control version of the task, m=1.0. The magnitude cue is present when $m \neq 0.5$. To explore the effect magnitude cue on C2PD performance, we stimulated C2PD at m = 0.5, 0.6, 0.7, and 1.0 (Fig. 3.2). As expected, the larger the magnitude factor, the higher the performance of the observer was (Fig. 3.2A). The above 50% proportion correct at 0.0c separation distance suggests that the Bayesian observer was taking advantage of the magnitude cue in addition to the spatial cue to make a decision. To study the effect of the magnitude cue along on perceptual performance, we simulated a non-Bayesian total-spike-count decoder that ignored the spatial pattern of the neural activity. This total-spike-count decoder makes decisions by comparing the 2-point

and 1-point stimulus intervals' total spike count; it simply selects the interval with a greater total spike count as the 2-point stimulus interval. As shown in Fig. 3.2B, higher magnitude factors resulted in progressively better performance of the total-spike-count decoder. Because this decoder did not have access to spatial information, performance was not impacted by stimulus separation distance, resulting in a horizontal plot. The excellent performance of this decoder as the magnitude cue approaches 1.0 supports previous empirical research that has called into question the validity of C2PD as a means of measuring tactile spatial acuity.

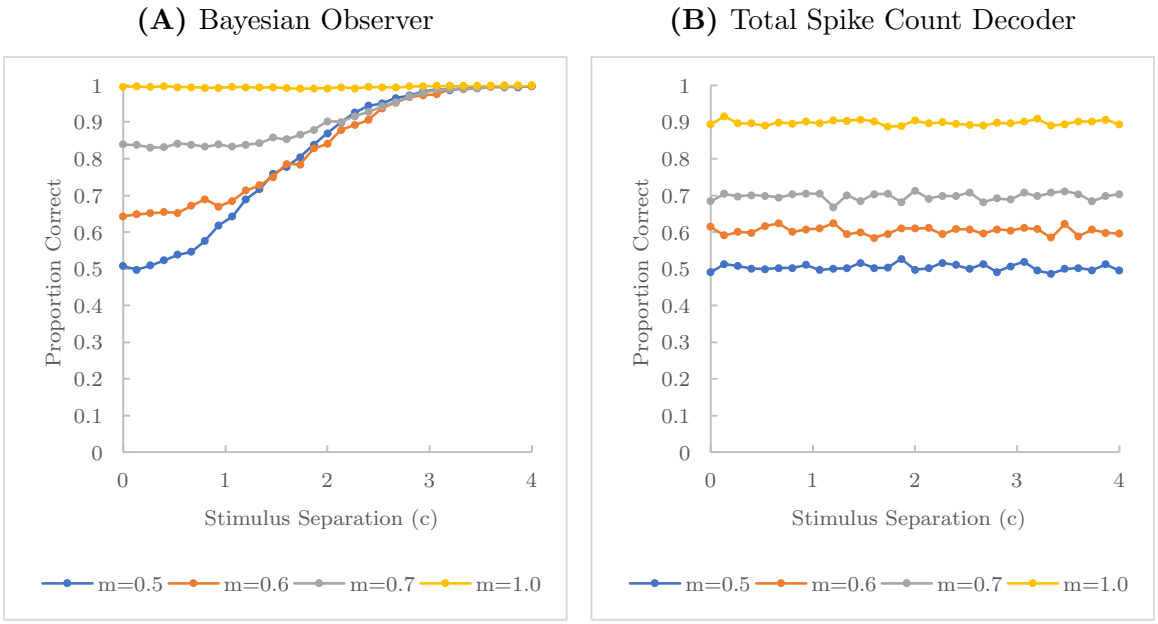

Figure 3.2: The Effect of Magnitude Cue on C2PD. Bayesian observer's and total-spike-count decoder's performance at different stimulus separation distances for C2PD at varying magnitude cue strength. The simple decoder considers the interval with the higher number of action potentials as the two-point stimulus interval

3.3 Intensity vs Threshold

The effect of intensity on the performance across 2PD tasks, under the force-control paradigm, was as expected. Increasing stimulus intensity resulted in higher performance and lower 76% correct thresholds. We used linear interpolation to measure the 76% threshold. Our default force-control point-stimulus intensity was $I_V = 0.5$ and $I_O = 1.0$. By increasing the stimulus intensity by a factor of 1.5 and 2, we obtained Fig.3.3. Once again, the S2PD (76% threshold 0.31c, 0.22c, 0.18c) outperformed 2POD (76% threshold 1.32c, 1.08c, 0.96c) and C2PD (76% threshold 1.52c, 1.27c, 1.13c) tasks at all intensity levels. Interestingly, the increase in the stimulus intensity resulted in a diminishing improvement in performance across tasks. To test whether the increase in performance as the result of an increase in stimulus intensity is asymptotic, we use the Bayesian adaptive method to explore the effect of stimulus intensity of up to 100 on the performance. As shown in Fig.3.3D, the increase in performance (the decrease in threshold) seems to be asymptotic.

3.4 S2PD vs C2PD vs 2POD

So far, we have shown that under the force-control paradigm, the performance of S2PD is consistently higher than 2POD and C2PD. The reason behind this performance difference can be better illustrated by comparing the spike count profile for each task's intervals. The spike count profile is a matrix that shows the action potentials fired by each neuron in the encoder. As expected, under the force-control paradigm, the average spike count profile of all tasks and their intervals are identical (Fig.3.4A). However, as we increase the separation distance, the spatial profiles of

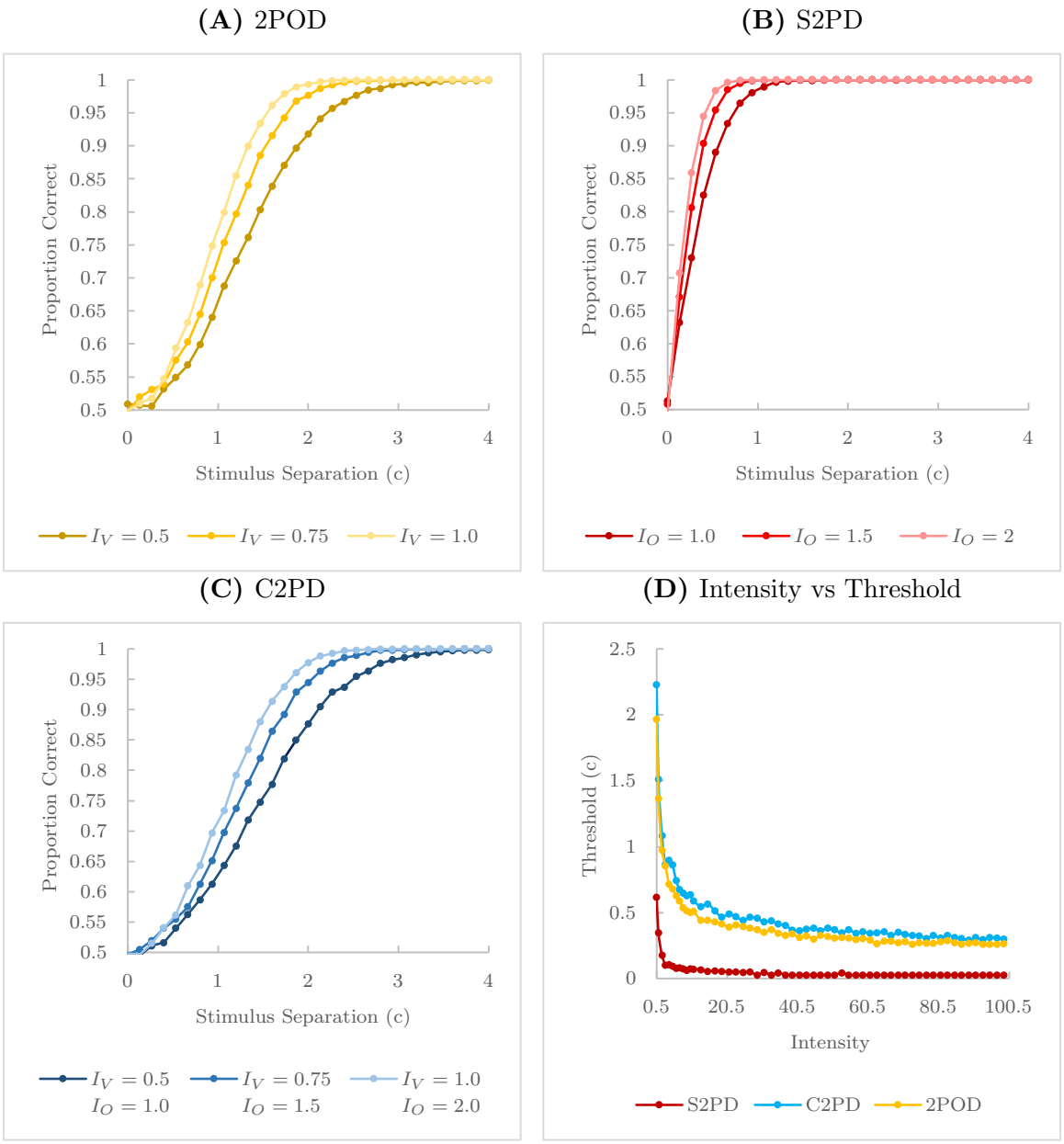

Figure 3.3: The Effect of Intensity on 2PD Tasks Performance. The Bayesian observer's proportion correct versus stimulus separation distance at varying intensity level for 2POD(**A**), C2PD (**C**), and S2PD (**B**) under force-control paradigm. (**D**) Increasing intensity resulted in lower threshold; however, the threshold asymptotes at high intensity levels.

the spike counts become distinguishable. The decoder is tasked with distinguishing the two intervals. The more similar the spatial spike count profiles are, the lower the performance of the decoder on the task. When looking at the activity profiles at 2c separation, the intervals of S2PD look most distinguishable from each other compared to the intervals of other tasks (Fig.3.4B). At 4c separation, all the activity profiles look very distinct, which could explain the ∼100% performance of the 2PD tasks at high separation distances.

3.5 The Effect of Sigma

We investigated the effect of varying the receptive field width, σ, on 2PD tasks performance (Fig. 3.5). We tested three σ levels, $\frac{2}{3}c, c, \frac{3}{2}c$. We used linear interpolation to find the 76% threshold. In C2PD, the 76% threshold was measured to be 1.19 for $\sigma = \frac{2}{3}c$, 1.50 for $\sigma = c$, and 1.71 for $\sigma = \frac{3}{2}c$. In 2POD, the 76% threshold was measured to be 1.07 for $\sigma = \frac{2}{3}c$, 1.32 for $\sigma = c$, and 1.50 for $\sigma = \frac{3}{2}c$. In S2PD, the 76% threshold was measured to be 0.32 for $\sigma = \frac{2}{3}c$, 0.31 for $\sigma = c$, and 0.31 for $\sigma = \frac{3}{2}c$. In C2PD and 2POD, decrease in σ levels corresponded to an increase in performance (Fig. 3.5A,3.5C); however, in S2PD, changes in σ levels did not affect performance (Fig. 3.5B). To investigate whether the variable impact of σ on 2PD tasks was due to the task setup or the variable baseline performance, we decided to normalize the 2PD tasks. We adjusted the intensity of 2POD and S2PD such that their 76% threshold coincides with C2PD threshold. After normalizing the tasks, 2POD performed similarly to C2PD; however, S2PD performed better than the other tasks at separations below the threshold and performed worse at separations above the threshold. We also looked at how varying σ from $0.3c$ to $2c$ in increments of $0.6c$ affects 2PD

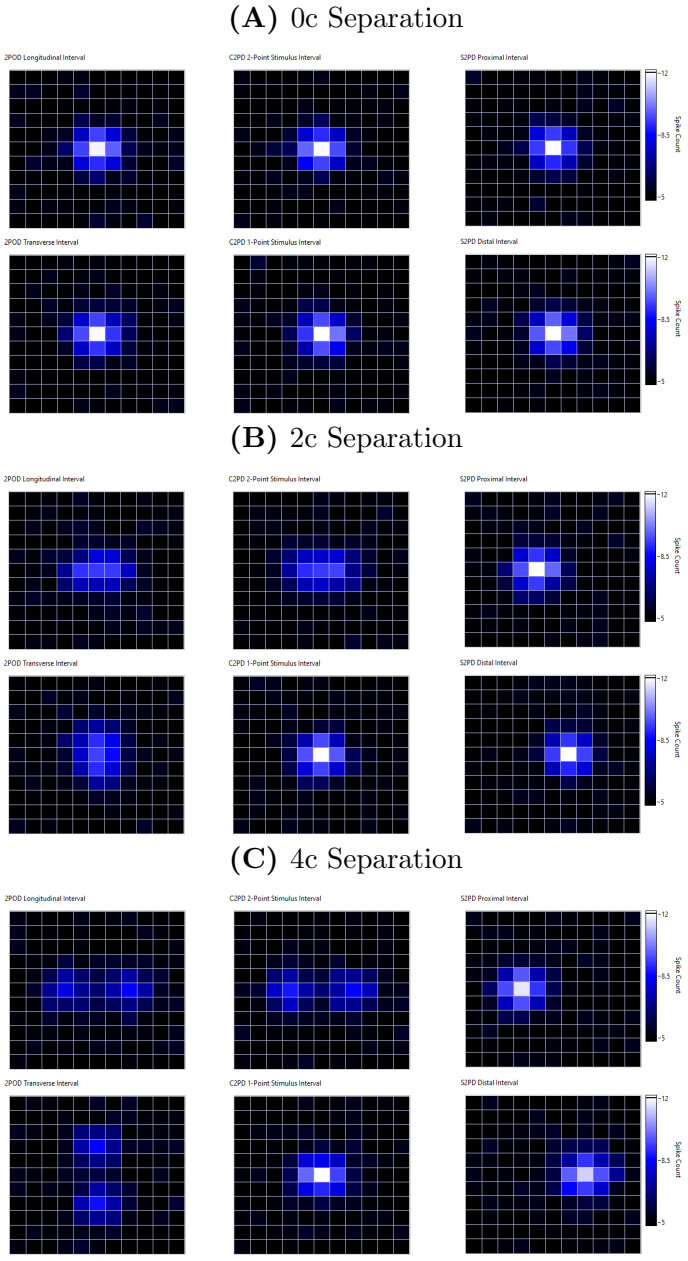

Figure 3.4: 2PD Spike Count Profile. The encoder spike count profile at various separations and across tasks and intervals, under force-control paradigm. Each cell represents a neuron in which the color of the cell indicates the number of action potentials it fired due to the stimulus. The brighter the color, the higher the number of action potentials. At 0c separation **(A)**, all the spike count profiles look identical to each other. At 2c separation **(B)**, it is much easier to distinguish between profiles. At 4c separation **(C)**, each profile looks very distinct.

performance. As shown previously, the performance of C2PD and 2POD worsened by increasing sigma levels and the performance S2PD remained the same. Next, we looked at how these trajectories changed when we normalized the tasks. Under the normalized conditions, the 2POD had the same trajectory as C2PD. Contrastingly, the performance of S2PD improved by increasing sigma levels at lower sigma values and asymptoted to $1.24c$ at higher sigma values. These trends suggest that with high sigma values the performance of S2PD does not change with increasing sigma values.

3.6 Duplication Factor

We explored how our model performs if we increase the number of cortical neurons that independently sample from the receptive field. Each of the original neurons in our grid (such as the 11 x 11 neuron grid of Figure 2.1B) is duplicated ($D = 2$) or quadrupled ($D = 4$), such that 2 or 4 (or etc) neurons occupy the identical location and respond independently to the stimulus. Thus, we tested duplication factors $D = 1, 2, 4$. Across all 2PD tasks, increasing the duplication factor increased the performance of the Bayesian observer on the task. In 2POD, the thresholds when D = 1,2, and 4 are 1.32, 1.09, and 0.90 accordingly (Fig. 3.6A). In S2PD, the thresholds are 0.31, 0.22, and 0.15(Fig. 3.6B). In C2PD, the thresholds are 1.50, 1.25, and 1.04 (Fig. 3.6C). Using the Bayesian adaptive method, we determined the 76% threshold at duplication factors from 1 to 1024.

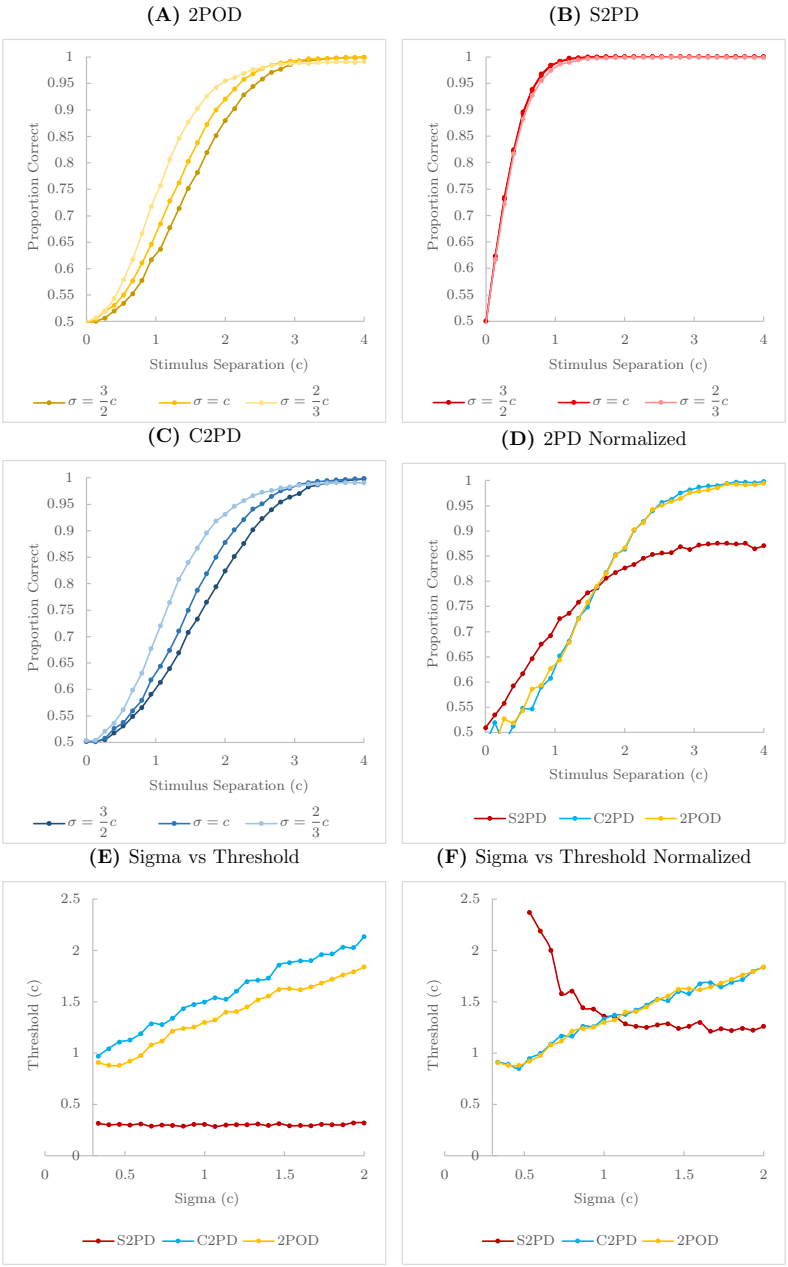

Figure 3.5: The Effect of Sigma on 2PD Tasks Performance. The impact of different sigma levels on the Bayesian observer's proportion correct versus stimulus separation distance for 2POD(**A**), S2PD(**B**), and C2PD(**C**) under force-control paradigm. C2PD(**D**) The intensity of 2POD was reduced by 22% and the intensity of S2PD was reduced to 81% in order for to have a similar 76% threshold to C2PD. **(E)** Increasing the sigma level resulted in a lower threshold for 2POD and C2PD tasks and had negligible effect of S2PD performance.(**F**) Under the normalized condition, the performance of 2POD and C2PD were similar and positively correlated with sigma level. S2PD did not have a 76% threshold at $\sigma = 0.3c, 0.4c, or 0.47c$. The performance on S2PD increased with increasing sigma level until it intersected the other two 2PD tasks at $1.3c \pm 0.3$, after which, it asymptoted.

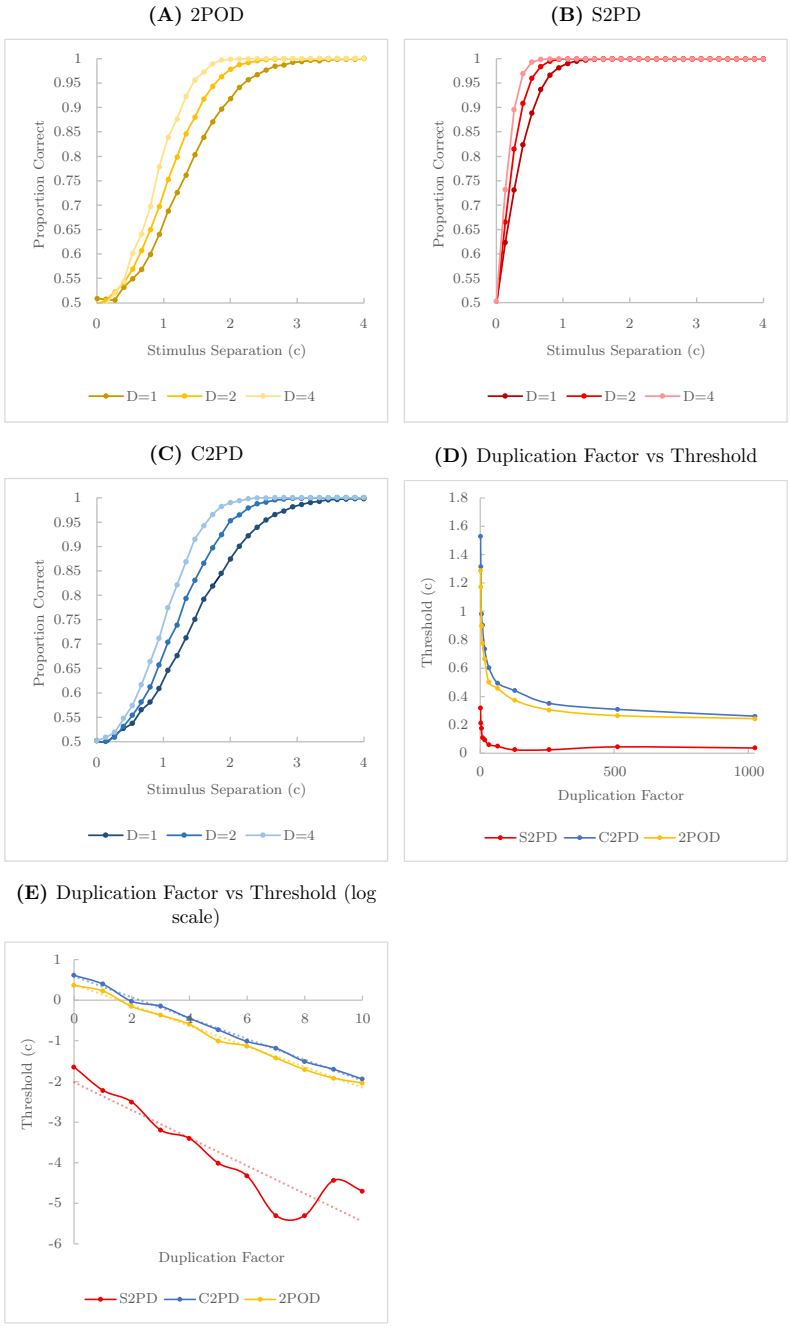

Figure 3.6: The Effect of Duplication Factor on 2PD Tasks Performance. The impact of different duplication factor on the Bayesian observer's proportion correct versus stimulus separation distance for **(A)** 2POD, **(B)** S2PD **(B)**, and C2PD **(C)** under force-control paradigm. **(D)**Increasing the duplication factor resulted in a lower threshold for all 2PD tasks.**(E)** On the log scale, the 2PD plots show a linear trend, with C2PD having a slope of -0.26, 2POD having a slope of -0.25, and S2PD having a slope of -0.34.

3.7 Jitter Awareness

We investigated the effect of jittering RF characteristics on model performance, and we examined conditions in which the decoder was or was not aware of the jitter (Fig. 3.7). At both jitter levels (J=2, J=4), the Bayesian observer's performance is impacted by the jittering and the awareness regarding RF characteristics. When J=5, jitter awareness made a greater difference. The average total spike count in no jitter condition for all 2PD tasks was 652 AP. The average total spike count in jitter conditions for all 2PD tasks was 806 AP. In 2POD and C2PD, being aware of jitter in the jittered condition had a higher performance at an early stimulus separation distance than in the no jitter condition, which can be explained by the higher total spike counts in the jitter condition than the no jitter condition.

3.8 Prediction

3.8.1 Circular Stimulus

Real psychophysical experiments use punctate stimuli, such as pinheads, that have a certain diameter. So far we have simulated our experiments assuming that the stimuli are points with no diameters. To investigate the effect on performance of the size of the stimulator, we simulated 2PD tasks with varying stimulus radii SR, $SR = 0, \frac{1}{3}, \frac{2}{3}$. We also ran these simulations under the force-control paradigm and under two new sub-paradigms, variable-indentation and fixed-indentation. The results—-shown in Figure 3.8— indicate that under variable-indentation sub-paradigm, the performance decreased as the stimulus radius increased. However, under the fixed-indentation sub-paradigm, the performance for S2PD increased with increasing stimulus radius. No

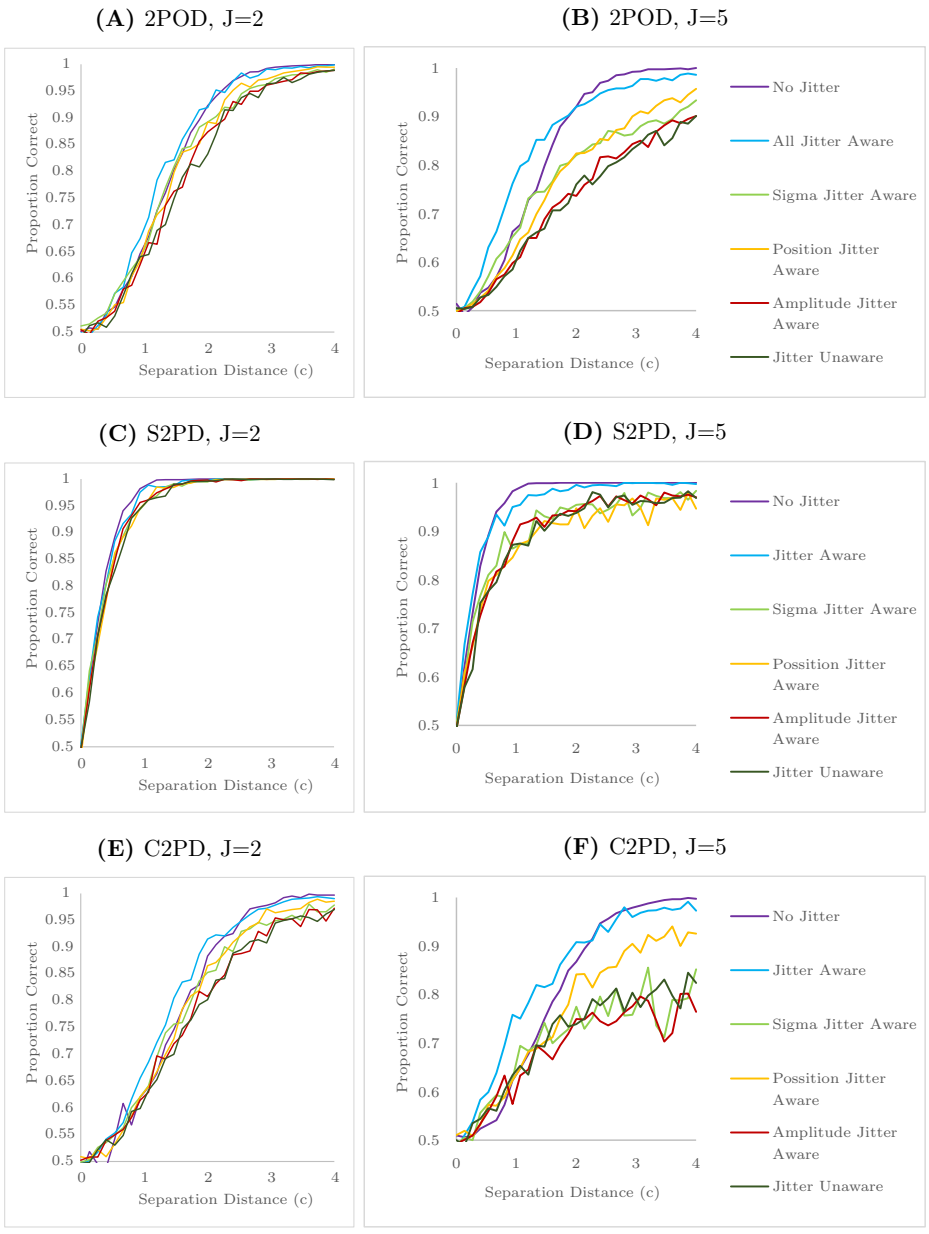

Figure 3.7: The Effect of Jitter on 2PD Tasks Performance. The impact of jitter on the Bayesian observer's proportion correct versus stimulus separation distance for 2POD **(A,B)**, S2PD **(C,D)**, and C2PD **(E,F)** under force-control paradigm. Except for the no jitter condition, in all other conditions σ,A, and c were jittered using equation 2.1.2.

pronounced pattern between performance and stimulus radius was observed in C2PD and 2POD under fixed-indentation sub-paradigm. These results make predictions that can be tested in future human psychophysics work.

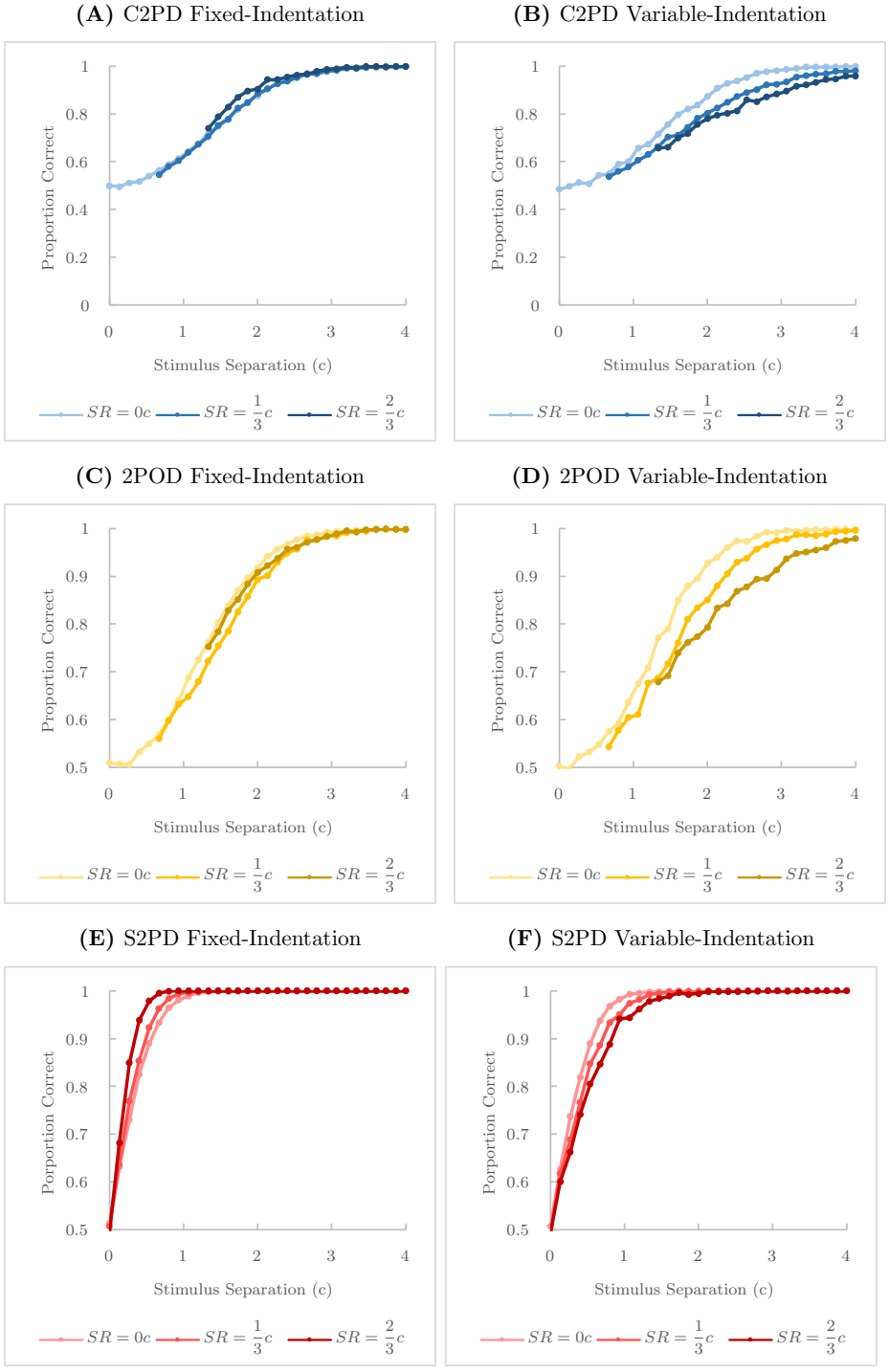

Figure 3.8: The Effect of Stimulus Radius on 2PD Tasks Performance. The impact of stimulus radius length on Bayesian observer's performance in 2PD tasks under fixed or variable indentation paradigm. Under the variable-indentation paradigm, the performance of 2PD tasks increased with increasing stimulus radius.

Chapter 4

Character Recognition Results

4.1 Letter Recognition Confusion Metrices

In addition to the two-point tests discussed in the previous chapter, raised-character identification tests have proved useful as measures of tactile spatial acuity in humans (Craig & Lyle, 2001; Essick et al., 1999; Johnson & Phillips, 1981b). Here, we simulate such tasks with our Bayesian observer model. The raised-letter recognition task confusion matrix data (Fig. 4.1) from Craig (1979) were used to simulate the experiment. The average hit rate of human participants on this task was 52%. We adjusted stimulus intensity such that the average hit rate of our simulation was also 52%. The Pearson correlation between the simulated and the experimental confusion matrix diagonals was 82%, and the whole matrix correlation was 94%. Similarly, we fit our observer's performance in the Braille character recognition task to the human participant hit rate from Loomis (1982). The average hit rate for both human participants and our simulation on this task was 61%. The Pearson correlation between the simulated and the experimental confusion matrix diagonals was 72%, and the

whole matrix correlation was 95%. We then compared the percent correct recognition for each letter by human participants to that of the Bayesian observer under the force-control paradigm (Fig. 4.2).

Having investigated the performance of the Bayesian observer on the Braille character recognition task under the force-control paradigm, we simulated this task under the displacement-control paradigm (Fig. 4.3). We were interested if the performance on the task would differ based on the experimental paradigm; in other words, we were interested in whether Braille reading strategy affects performance. The force-control paradigm can be analogous to tracing Braille characters by vertical finger movement (such that the force on the characters remains constant), whereas the displacement-control paradigm can be analogous to reading with a fixed vertical finger position. Poor Braille readers tend to have more variable vertical finger movement compared to skilled readers (Davidson et al., 1980; M. Heller, 1993; Nonaka et al., 2021; Papadimitriou & Argyropoulos, 2017). Although vertical finger movement in reading Braille does not necessarily indicate a force-control paradigm, the absence of vertical finger movement does indicate a displacement-control paradigm.

The Bayesian observer's average hit rate was fit to that of human participants by adjusting the stimulus intensity parameter. Under the displacement-control paradigm, the stimulus intensity had to be 77.4% smaller than that of the force-control paradigm to fit human participants, suggesting that the displacement-control paradigm is more informative than force-control. The Pearson correlation between the displacement-control simulated and the experimental confusion matrix diagonals was 53%, and the whole matrix correlation was 93%. The resultant confusion matrices of the two simulations—force-control and displacement-control—were comparable such that the

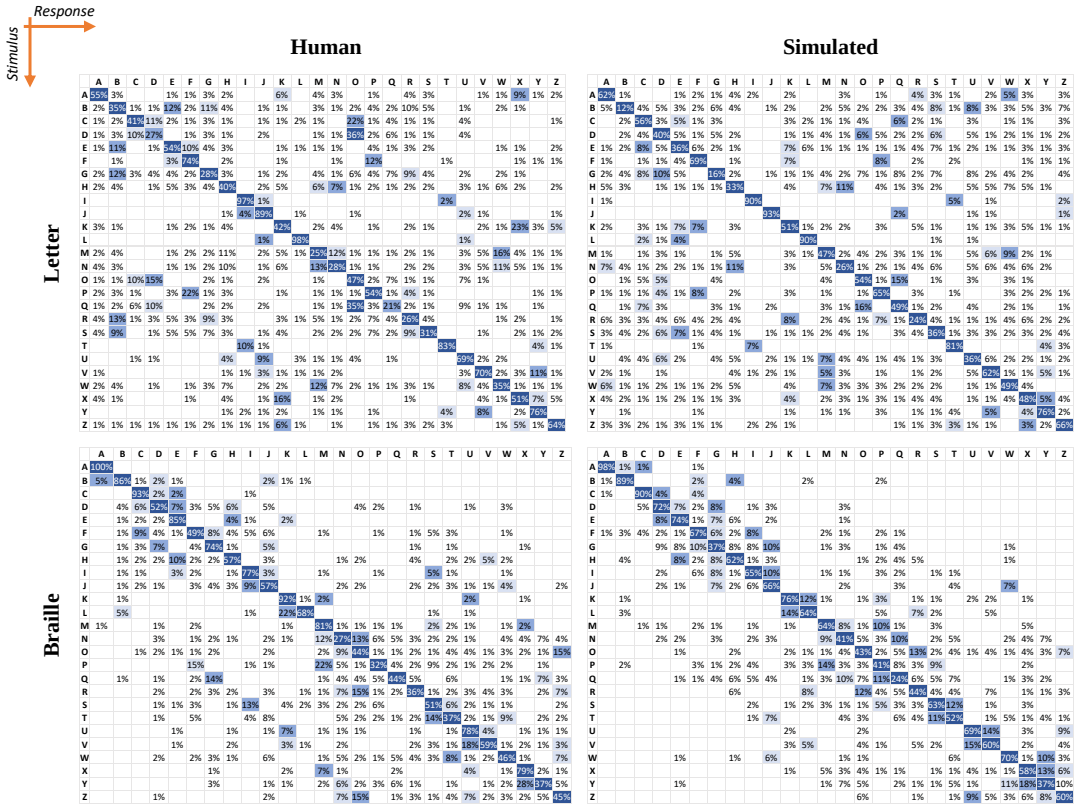

Figure 4.1: Character Recognition Task Confusion Matrices. Braille and raised-letter recognition task confusion matrices from human and simulated experiments. The human data for the raised-letter confusion matrix was taken from Craig (1979), and the human data for the Braille-character confusion matrix was taken form Loomis (1982). The simulated confusion matrices were created by adjusting the stimulus intensity parameter such that the average hit rate matched the human data. The top three highest response letters for a given stimulus are highlighted such that the highest response letter has a dark blue cell. Blank cells represent a value $< 0.5\%$.

(A) Braille Character

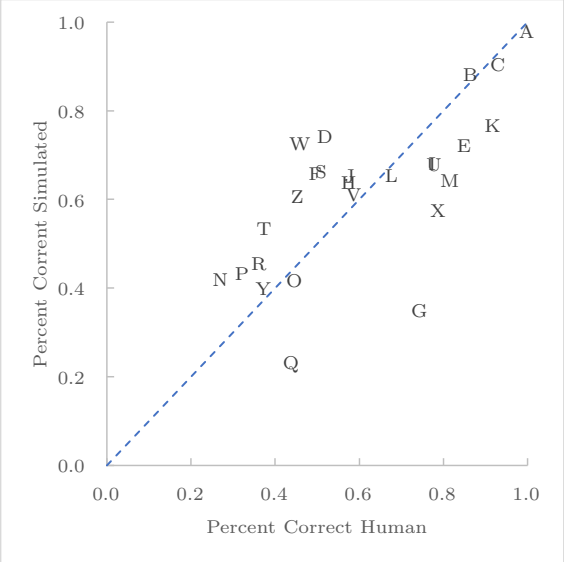

(B) Raisesd Letter

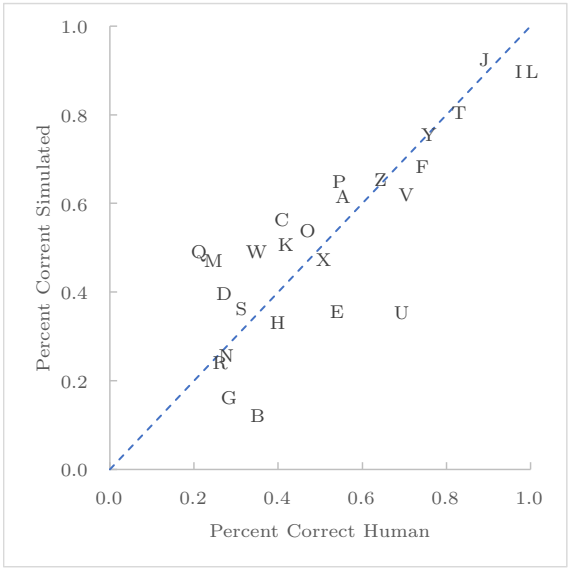

Figure 4.2: Character Recognition Tasks Hit Rate. The Bayesian observer's percent correct recognition for each letter vs the percent correct recognition by human participants in raised letter **(A)** and Braille character **(B)** recognition tasks.

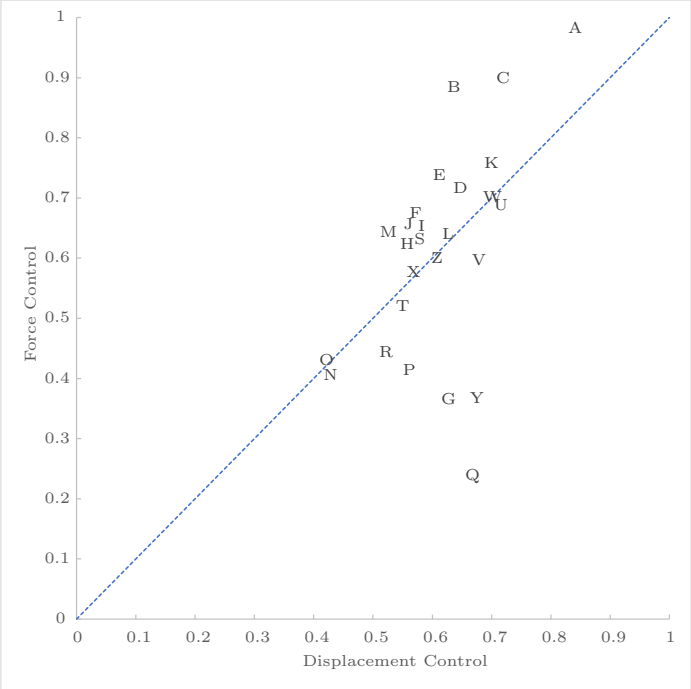

Figure 4.3: Braille Recognition Tasks Performance. The Bayesian observer's percent correct Braille character recognized under the force-control vs. the displacement-control paradigm.

Pearson correlation of confusion matrix diagonals was 52%, and the whole matrix correlation was 95%. Although many characters had a similar recognition accuracy under the two paradigms, there were some characters that did not. Mainly, characters with a smaller number of points (A, B, C) performed better under force-control, and characters with a high number of points (G, Q, Y) performed better under displacement-control (Fig. 4.3).

4.1.1 Most Confusing Letters

Having shown the similarity in correct recognition of each letters between humans and the Bayesian observer on RLRT (Fig. 4.2A), we were interested in comparing the incorrect stimulus-response pair recognition between the model and humans. We looked at the top twenty incorrect stimulus-response pairs (based on proportion response) for both the Bayesian observer and human participants (Table. 4.1). Interestingly, the stimulus-response pair percent recognition were not symmetrical for both the Bayesian observer and humans (i.e, the proportion response of D-O pair is different from O-D pair). Among this list, we can see similarities in letter confusion between the Bayesian observer and humans, such as rounded letters (D, O, Q) getting confused with one another. One major difference between the Bayesian observer and humans is that the proportion response of the top confused letters is lower in the Bayesian observer, suggesting that the incorrect recognition in the Bayesian observer is more uniformly distributed.

4.1.2 Letter Similarity

We were interested in whether letter similarity is correlated with an incorrect response in RLRT. Letter similarity was measured by quantified by measuring the Pearson correlation of between any two letters bitmap. We found that stimulus-response pair letter similarity was moderately correlated with proportion of incorrect responses in our simulation ($R = 0.59$) and weakly correlated in human participants ($R = 0.40$) (fig. 4.4).

Table 4.1: Most confused stimulus-response pair from Bayesian observer and human data (Craig, 1979) for the raised-letter recognition task.

Human Participant			Bayesian Observer		
Stimulus	Response	Proportion Response	**Stimulus**	Response	Proportion Response
D	O	35.70%	**Q**	O	16.16%
Q	O	34.50%	**O**	Q	15.40%
K	X	22.60%	**H**	N	11.36%
C	O	22.20%	**N**	H	11.00%
P	F	21.60%	**G**	D	10.20%
M	W	16.30%	**M**	W	8.64%
X	K	15.70%	**B**	U	8.44%
O	D	15.00%	**F**	p	8.44%
R	B	13.40%	**B**	S	8.20%
N	M	12.80%	**P**	F	8.08%
F	P	12.30%	**R**	K	7.92%
W	M	12.10%	**G**	C	7.76%
B	E	11.70%	**G**	Q	7.56%
G	B	11.60%	**E**	C	7.56%
M	N	11.60%	**G**	U	7.52%
C	D	11.10%	**K**	F	7.44%
E	B	10.80%	**Q**	C	7.40%
N	W	10.80%	**H**	M	7.28%
B	G	10.60%	**R**	P	7.08%
V	Y	10.50%	**G**	O	6.96%

(A) Bayesian Observer

(B) Human Participants

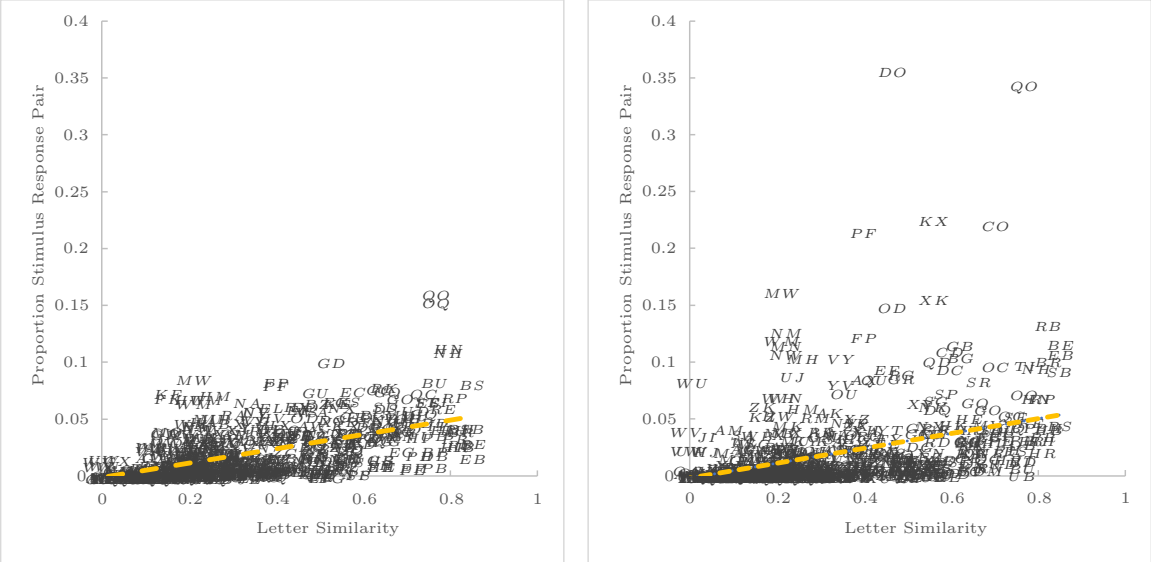

Figure 4.4: Braille Character Recognition Task Incorrect Responses. Proportion of incorrect response to a given stimulus vs stimulus-response letter similarity in Braille character recognition task. The first letter of the labels corresponds to the stimulus letter and the second letter corresponds to the response, so QO means responding O to the stimulus Q. The orange line is a linear trend line with $R = 0.59$ and slope of 0.063 for the Bayesian observer **(A)** and $R = 0.39$ and slope of 0.065 for human participants **(B)**.

4.2 Predictions

4.2.1 Ways To Make Braille Easier

The importance of the ability to read Braille is well documented (Hoskin et al., 2022); Braille literacy is correlated with employment, life-satisfaction, and self-esteem (Arielle Michal Silverman & Edward C. Bell, 2018; Ryles, 1996). Although the Braille literacy rate among blind individuals is not accurately known (Sheffield et al., 2022), some estimate that only 12% of blind individuals can read braille (Toussaint & Tiger, 2010). The estimated decline in Braille literacy rate from 50% in 1960s (Toussaint & Tiger, 2010) is alarming. Here, we looked at possible ways to improve Braille learning by increasing character recognition performance. specifically, we investigated at the effect of stimulus intensity and letter scaling on Braille character recognition performance. Under both force and displacement control paradigms, the increase in stimulus intensity and letter scale resulted in an increase in the average hit rate (Fig. 4.5). Unsurprisingly, the displacement control paradigm had higher performance due to the existence of magnitude cues. Our results suggest that Braille character recognition can be increased by increasing Braille height and inter-dot spacing.

4.2.2 The Effect of Masking

In studies of visual information processing, masking paradigms are often used to study the effect of "masking" stimuli on perceptibility of target stimulus (Breitmeyer & Ogmen, 2006). Visual lateral masking has shown to decrease performance in letter recognition tasks (Massaro & Klitzke, 1979). Similarly, Loomis and Apkarian-Stielau (1976) showed that lateral masking decreases the letter recognition in slit-scanning

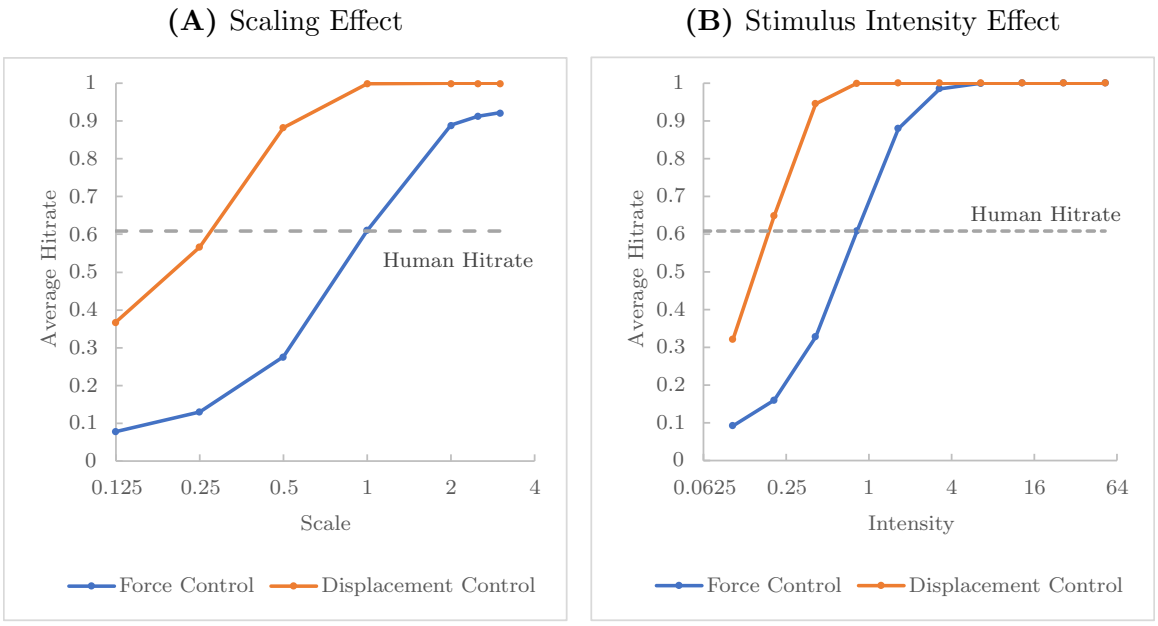

Figure 4.5: Braille Character Recognition Task Prediction. The effect of letter scale and stimulus intensity on the average hit rate on the Braille character recognition task under force and displacement-control paradigms.

condition, a condition in which letters are presented by moving through a stationary vertical slot at 16 columns/sec. They further showed that the distance of the masking stimuli to the target stimulus is correlated with the percent recognition. Inspired by their study, we investigated the effect of masking on the raised-letter recognition task when the letters are presented as a whole and in static condition (Fig. 4.6B). We used two columns of 14 points as our masking stimuli. In the no masking condition, the performance of the Bayesian observer was 52.6%. When the masking columns were at $\pm 3.7c$ and the decoder was aware of the masking stimuli, the average hit rate was 23.4%, but when the decoder was unaware of the masking stimuli, the average hit rate was 13.4%. When the masking columns were at $\pm 5c$ and the decoder was aware of the masking stimuli, the average hit rate was 26.2%, but when the decoder was unaware of the masking stimuli, the average hit rate was 17.2%. The total number of spike counts was the same in both far and near masking conditions.

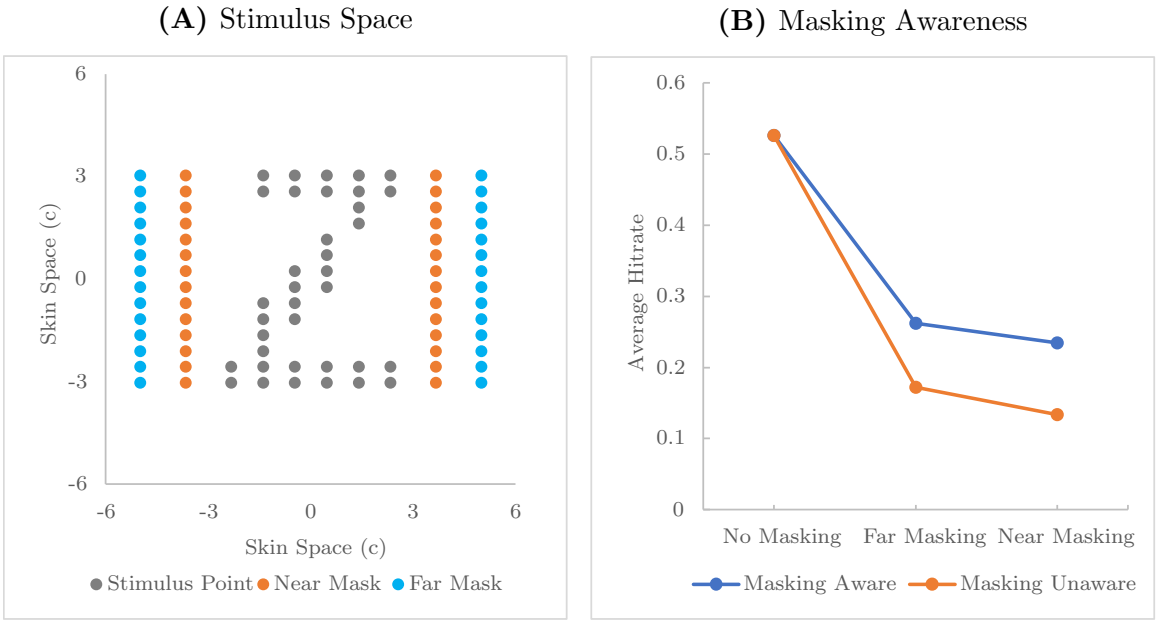

Figure 4.6: Raised-Letter Recognition Task Masking Prediction. The effect of masking on raised-letter recognition task performance. **(A)** The raised letter is shown as a series of punctate points at the center of the modelled skin space. Shown to the sides of the letter are the masking side bands that are comprised of two sets of 14 points. The near mask is at the horizontal position of $\pm 3.7c$ and the far mask is at the horizontal position of $\pm 5c$. **(B)** No masking condition has the highest performance followed by far masking and near masking conditions. Unawareness regarding the existence of masks further reduces performance.

Chapter 5

Illusion Tasks Results

5.1 Adaptation-Induced Repulsion Illusion

Inspired by the visual aftereffect illusion, in which lines are perceived as tilted away from an adapted orientation, Li et al. (2017) demonstrated an adaptation-induced repulsion illusion, in which stimulus is perceived as shifted away from an adapted area, in the sense of touch. In their study, they found that participants perceived the two-point stimulus separation to be larger when the area between the stimuli was adapted. Following their experimental procedure, we used skin parameters corresponding to the forearm. We simulated the presence of a tactile repulsion illusion on the model skin with and without an adaptor stimulus. In a AIRI task, the Bayesian observers compared the separation distance of a two-point stimulus on the reference hand to the comparison hand, reporting which distance was perceived greater. The reference distance was fixed at 2c, and the comparison distance varied from 0c to 4c. The point of subject equality (PSE) was extracted from the psychometric graphs as a measure of observers' perceived distance between the reference points. We measured

and compared the baseline PSEs and the PSEs under the adaptation paradigm.

Li et al. (2017) proposed that AIRI may be due to the brain's unawareness regarding its sensory neurons' adaptation. To investigate this claim, we simulated AIRI at different adaptation strength (α) and under adaptation-aware and unaware conditions (Fig. 5.1). In the adaptation-aware condition, the Bayesian observer knows the value of α and the effect of adaptation on the spike count. In adaptation unaware condition, the Bayesian observer assumes that there is no adaptation. As expected, when $\alpha = 0$, awareness regarding adaptation had no effect on the performance ($PSE = 2.00$). However, when the Bayesian observer was unaware of the adaptation while its neurons were adapted ($\alpha = 0.4\, and\, 0.8$), the PSE was shifted to the left ($PSE = 2.52\, and\, 3.25$). When the Bayesian observer was aware of the adaptation while its neurons were adapted ($\alpha = 0.4 and 0.8$), the PSE did not significantly change ($PSE = 1.97\, and\, 1.98$). Regardless of the Bayesian observer's awareness of adaption, adaptation lowered the slope of the psychometric functions due to the decrease in the signal-to-noise ratio. The PSE shift observed in the adaptation-unaware condition is because the Bayesian observer mistakenly interprets the lower firing rates of the adapted neurons to mean that the stimulus points are farther apart.

5.2 Orientation Anisotropy Illusion

Orientation anisotropy illusion was first discovered by Longo and Haggard (2011) in which stimulus separations on the dorsum of the hand are perceived larger when oriented transversely (across the hand) than longitudinally (along the hand). The authors suggested that this illusion arises from a mismatch between the representation of hand shape in the brain and in reality. To investigate their suggestion, we

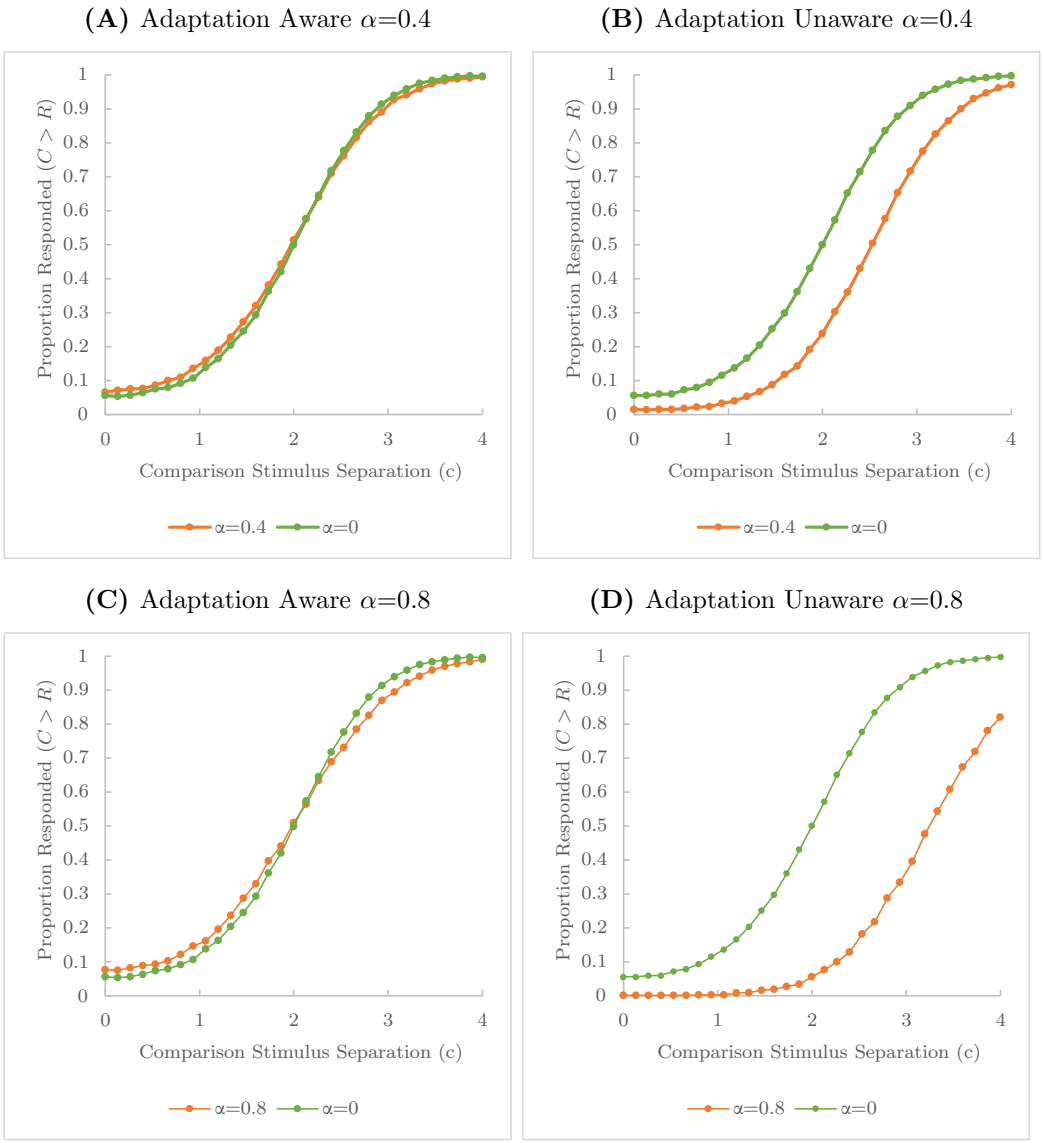

Figure 5.1: AIRI Adaptation Awareness. The proportion of times the Bayesian observer reported comparison stimulus separation is larger than the reference stimulus separation distance ($R = 2c$). The adapting stimulus was placed at the center of the skin patch. The awareness of the decoder regarding the adaptation state when there was no adaptation (α=0) was inconsequential and the $PSE = 2.00$. **(A)** When the decoder was aware of the adaptation ($\alpha = 0.4$), the $PSE = 1.97$, and **(B)** when the deocder was unaware of this adaptation, the $PSE = 2.52$. **(C)** When the decoder was aware of the adaptation ($\alpha = 0.8$), the $PSE = 1.98$, and **(D)** when the decoder was unaware of this adaptation, the $PSE = 3.25$;

first examined how the RFs in the dorsum and the palm of the hand differ. Significant peripheral afferent RF shape anisotropy is observed in the dorsum of the hand (Johansson & Vallbo, 1980). To determine whether RF shape anisotropy is true regarding cortical neurons, we looked at Merzenich et al. (1987) which used extracellular recording to map neuronal receptive fields in cortical areas 3b and 1. Using PlotDigitizer, we extracted RF dimensions and spacing (Fig. 5.2). Although we were able to extract information regarding the RF dimensions in the palm and dorsum of the hand, we were able to gather information for RF spacing only for the palm of the hand. Because we could not find information regarding RF spacing at the dorsum of the hand, we assumed that the cortical RF area overlap is the same on the palm and the dorsum of the hand. With this assumption, we were able to come up with RF spacing, such that the $\frac{\sigma_{ratio}}{c_{ratio}}$ is the same for both dorsum and palm of the hand. σ_{ratio} is the ratio of transverse sigma to longitudinal sigma, and c_{ratio} is the ratio of transverse RF spacing to longitudinal RF spacing. On the palm of macaque monkey hand, we measured the RF spacing ratio as 0.81 and the sigma ratio as 0.54. On the dorsum of the hand, we measured the RF spacing ratio to be 0.68 and the sigma ratio to be 0.45. Using these values, we updated our encoder to reflect the new RF tuning characteristics.

Next, we investigated how the observer's awareness of the RF properties affects their perception in the OAI (Fig. 5.3). When the Bayesian observer was aware of the RF anisotropy, the decoder's understanding of the modelled skin matched the encoder's modelled skin. When the Bayesian observer was unaware of the RF anisotropy, the decoder assumed that $\sigma_{ratio} = c_{ratio} = 1.0$. In the RF anisotropy-aware condition, the psychometric function for the palm (PSE = 1.86) and the dorsum (PSE =

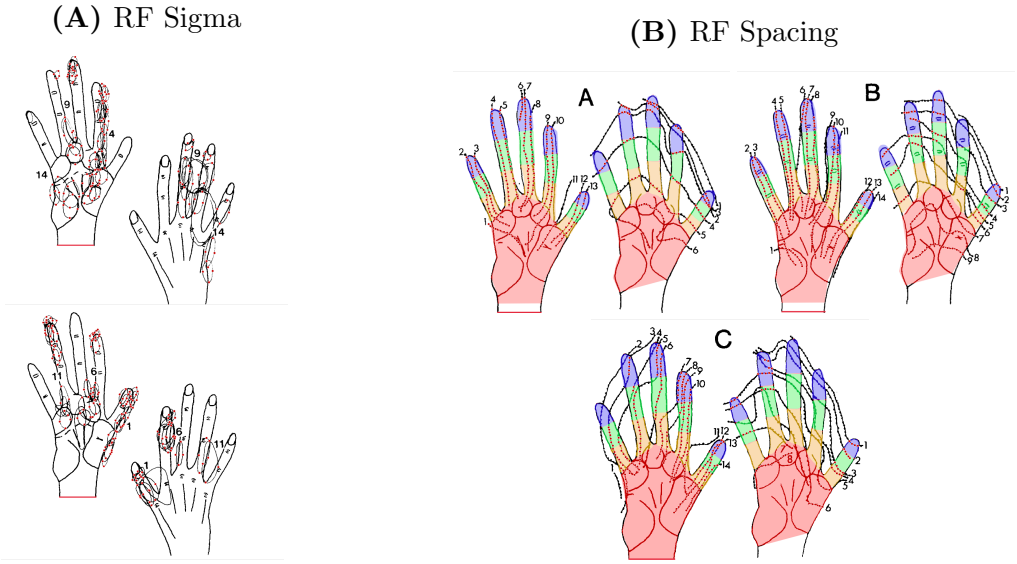

Figure 5.2: RF Sigma and Spacing Schematic. The RF spacing and sigma were extracted from Merzenich et al. (1987), which recorded the neuronal activity from cortical areas 3b of adult owl monkeys. **(A)** Examples of the RF map on the dorsum and palm of the hand. The area 3b and 1 cortical RFs are shown as ovals. By dividing the transverse diameters of these ovals by their longitudinal diameters, we measured the RF sigma ratio. The average sigma ratio of the RFs on the palm of the hand was measured to be 0.54 and on the dorsum of the hand was measured to be 0.45. **(B)** Examples of RF centers on the palm of the hand. The red dots are the RF centers that were used to measure inter-receptive field center spacing. By dividing the length of longitudinal RF spacing by the transverse RF spacing, we measured the RF spacing ratio. The average spacing ratio of the RFs on the palm of the hand was measured to be 0.81, and the average spacing ratio of the RFs on the dorsum of the hand was calculated to be 0.68.

1.85) were very similar to each other. In the RF anisotropy-unaware condition, the psychometric function for the dorsum of the hand (PSE = 1.41) was to the left of the psychometric function for the palm of the hand (PSE = 1.68), resulting in orientation anisotropy illusion.

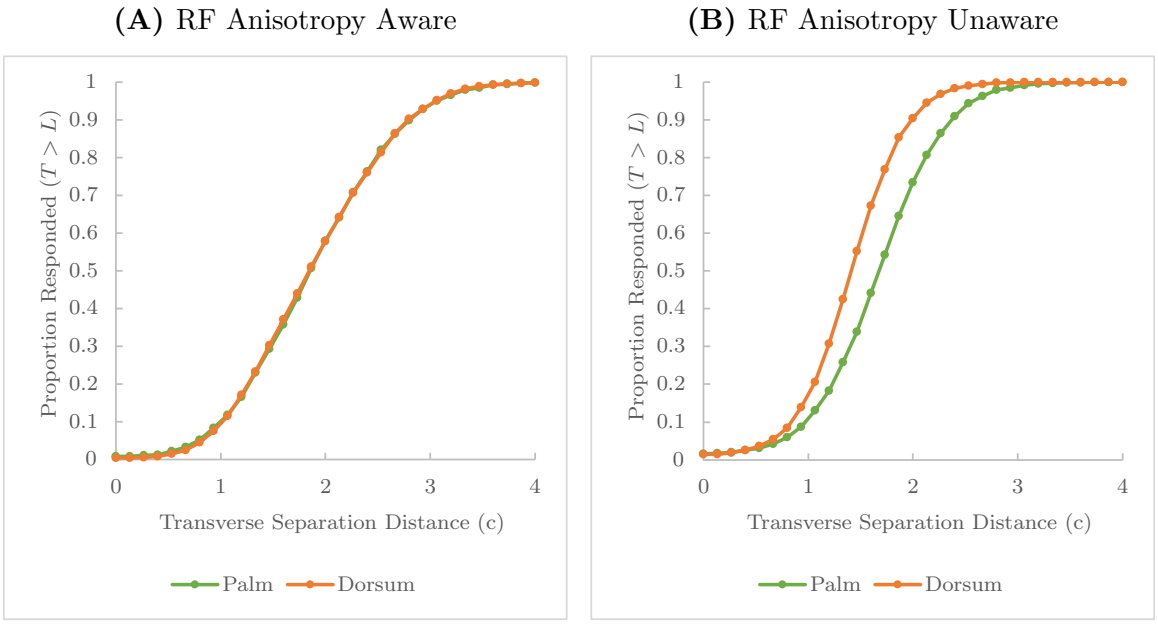

Figure 5.3: RF Anisotropy Awareness. The proportion of times the Bayesian observer reported transverse stimulus separation is larger than the longitudinal stimulus separation distance ($R = 2c$). **(A)** When the decoder was aware of the RF anisotropy and tested on the palm of the hand, $PSE = 1.86$, and when tested on the dorsum of the hand, $PSE = 1.85$. **(B)** When the decoder was unaware of the RF anisotropy and tested on the palm of the hand, $PSE = 1.68$, and when tested on the dorsum of the hand, $PSE = 1.41$.

5.3 Prediction

5.3.1 AIRI Surround Adaptation

The predecessor to AIRI is tactile spatial aftereffect as demonstrated by Day and Singer (1964). In their study, they showed that the separation distance between two stimulus bars is perceived as longer when the area between the bars was adapted, and the separation distance between two stimulus bars is perceived as shorter when the areas outside of the bars were adapted. However, their study contained methodological bias from using an asymmetrical range of comparison stimuli as pointed out by Day and Singer (1964). Although Li et al. (2017) demonstrated that adaptation of the area between stimuli results in spatial repulsion, it has remained open to investigation whether adaptation of the area outside stimuli results in spatial contraction. Therefore, we investigated what would happen if the adapting stimuli in AIRI were on the flanks of the skin patch (Fig. 5.4). The adapting stimuli with $SR = \frac{1}{15}c$ were placed at x =-3c and +3c positions of the skin patch. When the Bayesian observer was aware of adaptation, the adaptation of $\alpha = 0.4$ resulted in a PSE shift of $-0.02c$ and the adaptation of $\alpha = 0.8$ resulted in a PSE shift of $-0.04c$. When the Bayesian observer was unaware of adaptation, the adaptation of $\alpha = 0.4$ resulted in a PSE shift of $-0.11c$ and the adaptation of $\alpha = 0.8$ resulted in a PSE shift of $-0.29c$. Therefore, we predict that adaptation of regions outside of the stimulus leads to length contraction. We think the principle behind length contraction is similar to that of AIRI in that the decoder mistakenly interprets the lower firing rates of the adapted neurons at the surrounding regions of the skin to mean that the stimulus points are farther from those neurons and closer to the center of the skin patch.

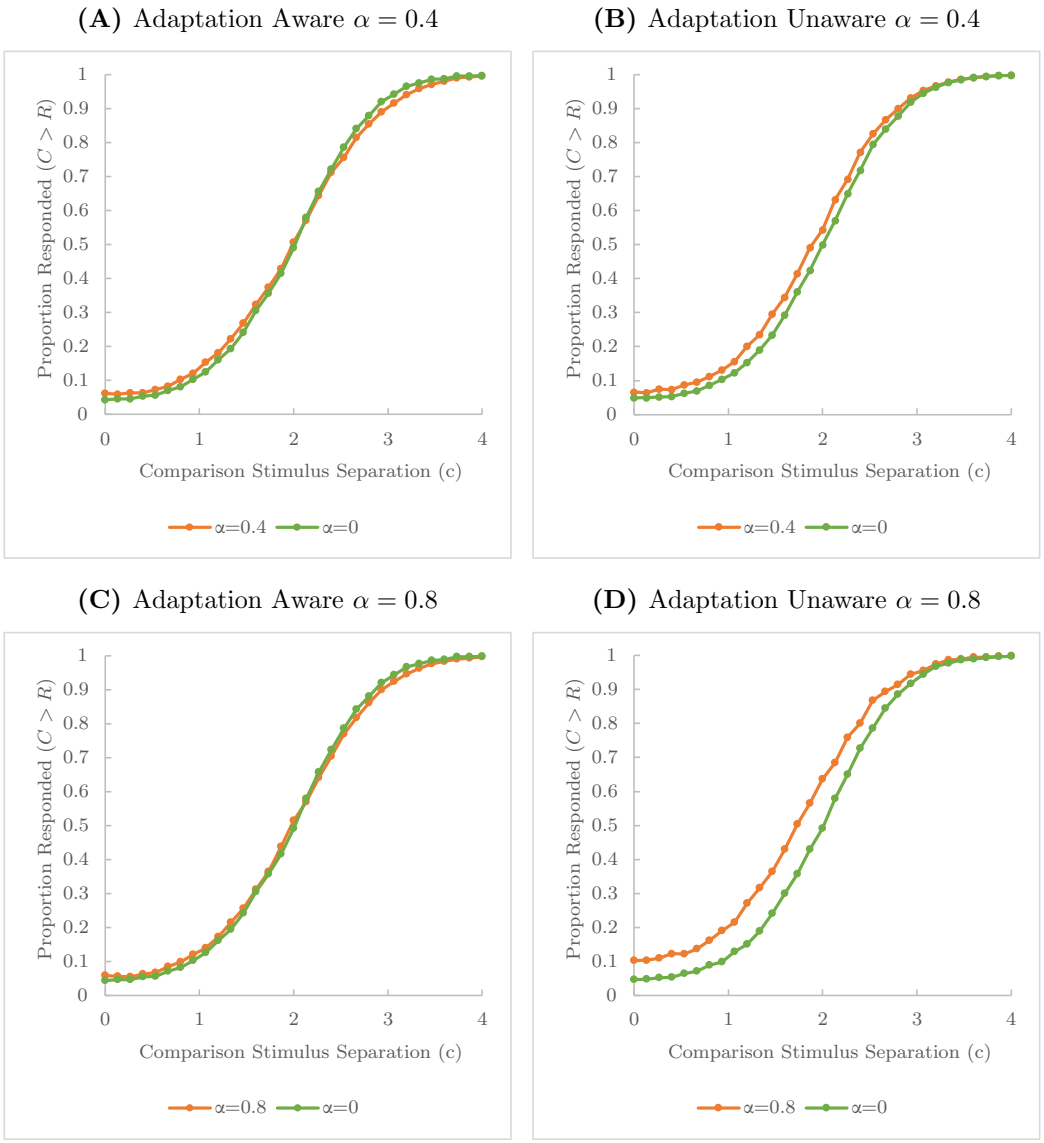

Figure 5.4: AIRI Surround Adaptation. The proportion of times the Bayesian observer reported comparison stimulus separation is larger than the reference stimulus separation distance ($R = 2c$). To stimulate surround adaptation, we placed adapting stimuli at $(-3c, 0c)$ and $(+3c, 0c)$. **(A)** When the decoder was aware of the $\alpha = 0.4$ adaptation, the $PSE = 1.99$, and when there was no adaptation, the $PSE = 2.01$. **(B)** When the decoder was unaware of the $\alpha = 0.4$ adaptation, the $PSE = 1.89$, and when there was no adaptation, the $PSE = 2.00$. **(C)** When the decoder was aware of the $\alpha = 0.8$ adaptation, the $PSE = 1.97$, and when there was no adaptation, the $PSE = 2.01$. **(D)** When the decoder was unaware of the $\alpha = 0.8$ adaptation, the $PSE = 1.73$, and when there was no adaptation, the $PSE = 2.01$.

5.3.2 OAI Oblique Stimulus

Having investigated the possible cause of OAI, we were next interested in whether using oblique stimulus instead of transverse or longitudinal stimuli would result in OAI. For this simulation, we followed the same procedure as in the default OAI simulation with the difference of using oblique two-point stimuli instead of transverse or longitudinal stimuli. In one interval, the observer is given a two-point stimulus oriented at $+45^\circ$ to longitudinal with a variable separation distance. In another interval, the observer is given a two-point stimulus oriented at -45° to longitudinal with a fixed 2c separation distance. As shown in Fig. 5.5, using oblique stimuli does not result in a shift of the psychometric curves, regardless of the observer's awareness of the RF anisotropy. For all conditions, the $PSE = 2.00$, which signifies that the observer does not experience OAI. That being said, unawareness of the RF anisotropy resulted in shallower curves, and the psychometric curves for the palm of the hand were shallower than the curves for the dorsum.

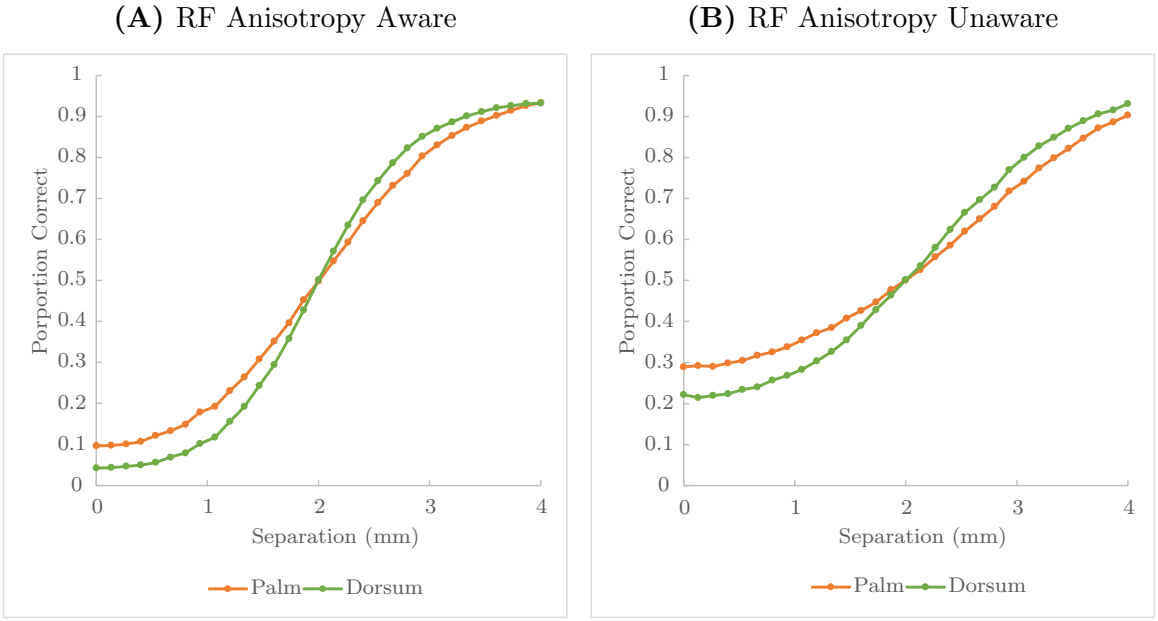

Figure 5.5: OAI Oblique Stimulus. The proportion of times the Bayesian observer reported whether the $+45°$ oblique stimulus separation is larger than the $-45°$ oblique stimulus separation distance ($R = 2c$). **(A)** When the decoder was aware of the RF anisotropy, the $PSE = 2.00$ on both the dorsum and palm of the hand; however, the slope of the psychometric plot for the dorsum was steeper than the one for the palm of the hand. **(B)** Similarly, when the decoder was unaware of the RF anisotropy, the $PSE = 2.00$ on both the dorsum and palm of the hand, and the slope of the psychometric plot for the dorsum was steeper than the one for the palm of the hand.

5.3.3 OAI Different Sigma and Spacing Ratios

Having investigated the decoder's awareness of the RF anisotropy in the palm and dorsum of the hand in OAI, we were next interested in how different sigma and spacing ratios affect perception (Fig. 5.6). We predict that OAI can be observed in the areas of skin where its RFs are anisotropic; the higher the RF anisotropy, the more pronounced the illusion. Specifically, we predict that a low c_{ratio} and a high σ_{ratio} will

result in a PSE shift to the left, and a high c_{ratio} will result in a positive PSE shift. Furthermore, when $c_{ratio} = \sigma_{ratio}$, increasing their ratios results in a rightward PSE shift.

(A) RF Anisotropy Aware

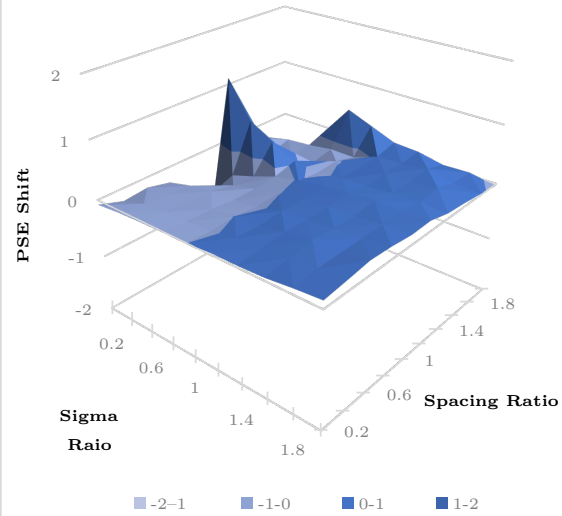

(B) RF Anisotropy Unaware

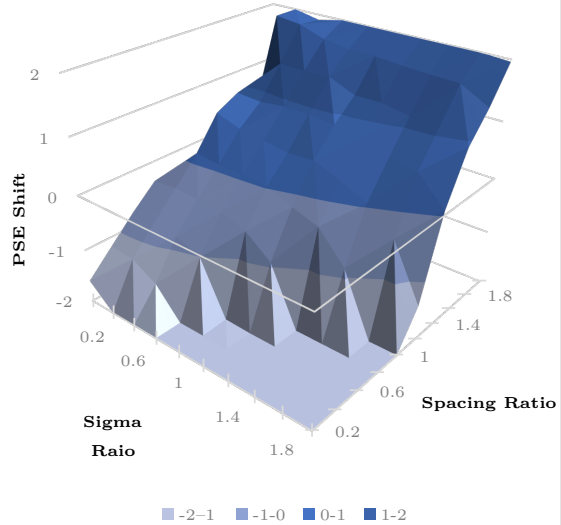

Figure 5.6: The Effect of Sigma and Spacing Ratio of PSE Shift. **(A)** The decoder was aware of RF sigma and spacing anisotropy. **(B)** The decoder was unaware of RF sigma and spacing anisotropy.

Chapter 6

Discussion

6.1 Two-Point Discrimination Tasks

The simplest form of assessing tactile spatial acuity is through a single-point localization test. In this test, the participants are asked to determine the location of the stimulus on their skin. In one variation of this task, the participants are instructed to close their eyes while being stimulated and open their eyes afterward to indicate the location of the stimulus by pointing to it with their finger (Yoshioka et al., 2013). Localization errors are then used to calculate a participant's threshold. Although simple to test, the validity of this method is questionable. The localization error is not only influenced by tactile spatial acuity but also by the participant's memory and motor localization. In a less problematic variation of the single-point localization test, participants are stimulated at a reference location and then subsequently stimulate at either the same or a different location. The participants are then asked to report whether the stimulus location remained the same or changed. By varying the distance of the second stimulus to the reference location, the participant's threshold

is calculated (Weinstein, 1968). A limitation of this task is that it is dependent on the criterion participants adopt for responding to what they perceive as "same" versus "different" locations. The two-point discrimination variation of this task, S2PD, mitigates the criterion issue as the participants understanding of proximal and distal location is irrelevant when the experiments is performed under 2IFC protocol.

The C2PD is often used in assessing tactile spatial acuity; however, the validity of this task has been called into question (Craig & Johnson, 2000; Johnson & Phillips, 1981b; Lundborg & Rosén, 2004). We can broadly categorize the C2PD's shortcomings into two components, experimental and fundamental. For this task to be valid, the total number of action potentials send to be brain must be the same between one-point intervals and two-point intervals with zero c separation. We call this a force-control paradigm based on the idea that the total force applied in a given interval remains constant. To ensure that there is no magnitude cue when running this task, the experimenters must consider the skin-stimulus dynamic and local circuitry when deciding the appropriate force for each stimulus point. The difficulty associated with finding the appropriate stimulus force level is an experimental shortcoming of C2PD. Under the force-control paradigm, C2PD is a valid task as the Bayesian observer's proportion correct at 0c separation is 50% (Fig. 3.1A). However, C2PD still has lower performance (higher threshold) than its alternatives (Fig. 3.1A), making it a less desirable task to use. Under the force-control paradigm, S2PD has higher performance (lower threshold) than 2POD and C2PD. The threshold in S2PD task was also lower than C2PD in human participants (Mancini et al., 2014). The low threshold of S2PD compared to the other 2PD tasks makes it a useful alternative in measuring tactile acuity on the fingertips (or other small skin areas).

If the experimenters use the same force for all individual stimulus points, then one would expect the number of action potentials in two-point intervals to be greater than the one-point intervals, under the linear summation of action potentials assumption. We called this experimental setup, the displacement-control paradigm, because it reflects the situation in which the depth of skin displacement is equal in the two intervals. Because of the unequal signal-to-noise ratio from each interval in displacement-controlled C2PD, the Bayesian observer can easily distinguish two-point from one-point intervals; hence, above 50% performance at 0c separation. In contrast, the displacement-control paradigm does not provide any magnitude cue advantage in S2PD and 2POD because the number of stimulus point(s) remain the same across their intervals.

Although magnitude cues can result from uncareful experimental procedures, they can also result from the sub-linear addition of neural responses. Studies in peripheral SA1 afferents have shown that closely spaced stimulus points suppress the neural response of each other (Vega-Bermudez & Johnson, 1999). Therefore, the number of action potentials created by two points is less than one point, resulting in a magnitude cue in C2PD. The magnitude cue resulting from the non-linear addition of neural responses is a fundamental shortcoming of C2PD. To illustrate the effect of the magnitude cue, we defined the magnitude factor as the intensity of a point in a two-point stimulus interval over the intensity of a point in a one-point interval. Varying the magnitude factor in C2PD (Fig. 3.2) resulted in above 50% performance, similar to results found in literature (Johnson & Phillips, 1981c; Tong et al., 2013). The magnitude cue is such an informative cue that our total spike count decoder had a relatively high performance at high magnitude factor values (Fig. 3.2B). Because

this decoder only took the total spike count into account, the performance remained constant across different stimulus separations.

6.1.1 S2PD is a Better Measure of Acuity

Under the force control paradigm, the total number of action potentials in a given interval of 2PD tasks are the same. So the total signal-to-noise ratio should also be the same, which begs the question of why the S2PD produces lower thresholds than 2POD and C2PD. To answer this question, we looked at the encoder spike count profile of all the 2PD tasks' intervals. At 0c separation, the profile of all the tasks looks the same. However, at 2c separation, the intervals in S2PD can easily be distinguished from each other in comparison to the other tasks. We think that the distribution of the signal is an important factor in explaining why S2PD had better performance. Similarly, 2POD intervals' spike patterns are more distinctive than C2PD intervals because of the orthogonal spread of action potentials in the 2POD transverse interval. At 4c separation, the intervals in all tasks can easily be distinguished.

6.1.2 Impact of Stimulus Intensity on Performance

SA1 mechanoreceptors are generally associated with tactile spatial resolution (Bruns et al., 2014). Their response is linearly correlated with indentation depth up to 1.5 mm (Mountcastle et al., 1966) and are only marginally impacted by indentation depths greater than 1.6 mm (Vega-Bermudez et al., 1991) or contact forces greater than 1 N (Johnson et al., 2000). Indentation depths greater than 1.6 - 1.8 mm results in saturation of SA1 afferents (Mountcastle et al., 1966). Thus, we may expect that tactile spatial acuity to be largely unaffected by the force of the stimulus after large

forces are reached (Vega-Bermudez & Johnson, 2004). Indeed, Johnson and Phillips (1981b) found that increasing indentation depth in the grating orientation task results in a diminished improvement in performance. G. O. Gibson and Craig (2006) showed that increasing stimulus force (from 50g to 200g) in the grating orientation task had no effect on performance. In this paper, we have also shown that increase in stimulus intensity resulted in diminished improvement in performance across all 2PD tasks (Fig. 3.3). Although the diminished performance in psychophysical studies could be attributed to the saturation of SA1 axons, given that we did not limit the number of action potentials in our model, our results suggest that there exists an irreducible source of spatial uncertainty that cannot be resolved by an increase in stimulus intensity.

6.1.3 Impact of RF Size on Performance

The RF size in many cortical areas has been shown to be malleable. Following digit amputation in adult owl monkeys, the size of RFs in un-amputated digits shrank (Merzenich et al., 1984). Following a focal lesion to the photoreceptor layer, the RFs in the cat's primary visual cortex expanded (Pettet & Gilbert, 1992). Lack of stimulation within the RF area paired with the stimulation surrounding the RF area resulted in RF size enlargement (Pettet & Gilbert, 1992). Peripheral denervation resulted in enlargement in RF size of raccoon's SI (Kaas et al., 1983). Gilbert and Wiesel (1992) found that following binocular retinal lesions, the RFs along the boundary of the lesion enlarged to five times their pre-lesion size. Moreover, cortical RF size can also alter due to experience-dependent plasticity. Womelsdorf et al. (2006) found that attention to stimulus position can shift rhesus macaque monkeys' cortical area MT RF centers

and shrink their RF size. Furthermore, the size of somatosensory cortical neuron RF varies across different body parts, which corresponds to their tactile acuity (Daroff & Aminoff, 2014). For example, the afferent neurons corresponding to the finger pad have relatively small Rfs, but their representation in the somatosensory cortex is large, corresponding with high tactile spatial acuity (Weinstein, 1968). Therefore, we predicted that the shrinkage of RF size would lead to improvements in performance.

To test this prediction, we looked at the effect of changing σ on 2PD task performance. Once again, S2PD had higher performance than 2POD and C2PD. However, the effect of σ was not the same across that tasks. In 2POD and C2PD, increasing the size of σ reduced performance, whereas, in S2PD, increasing the size of σ had negligible effect of the performance. By referring to the **Eq. 2.1.3**, we can see that increasing σ increases the expected stimulus-evoked spike count, s, of a neuron. Paradoxically, an increase in s does not necessarily increase performance; in fact, increasing σ lessens the contribution of stimulus distance to s. To make this point more clear, let us assume that $A = 10AP$, $I = 1$ and $\sigma = 15mm$. When $d = 0mm$, $s = 10AP$, and when $d = 15mm$, $s = 6AP$. Now let us consider the same case but with $\sigma = 50mm$. In this case, when $d = 15mm$, $s = 9.5AP$, which is similar to $s = 10AP$ at $d = 0mm$. Therefore, at high σ values, the Bayesian decoder has a harder time inferring the true distance of the stimulus because the expected stimulus-evoked spike count at different separations are similar to each other.

6.1.4 Duplication Factor

An important assumption in our model is that all the neurons' spike counts are conditionally independent of one another. However, neurons in the primary somatosensory cortex receive convergent inputs from many neurons in the network and output to many other neurons in a form of excitatory and inhibitory lateral connections (Doetsch et al., 1992; Kang et al., 1985; Macgillis et al., 1983; Xing & Gerstein, 1996). Application of GABA antagonists has been shown to enlarge the RF size of SI neurons (Alloway et al., 1989), which suggests that inhibitory connections affect tactile acuity by regulating RF size. Lateral inhibition is theorized to be an important process in refining somatosensory information and improving the discrimination of two points (Daroff & Aminoff, 2014). Xing and Gerstein (1996) attributes modulation in RF size of neurons in SI to excitatory and lateral connections in which RF sizes increase with an increase in excitatory levels and decrease with an increase in inhibitory levels. That being said, we can view each neuron in our model as a representation of a set of cortical neurons whose collective inputs are conditionally independent of other sets.

To explore what would happen if multiple neurons received the same input, we came up with a duplication factor. The duplication factor can be viewed as an independent sampling of the data. As expected, increasing the duplication factor increased the performance across all 2PD tasks (Fig. 3.6). Our result suggests that by having more neurons independently receive information from the peripheral afferent, tactile acuity performance increases. In fact, by having an infinite number of cortical neurons the performance would be equal to the performance if decoding happened in the peripheral neurons. A similar process could underlie improvement in tactile

acuity due to the enlargement of skin representation in the cortex. Merzenich et al. (1984) reported that cortical representation of digits increased upon amputation of an adjacent digit. This increase in representation was accompanied by an increase in tactile acuity. Meaning, by recruiting more neurons to attend to a particular skin area the brain could increase the tactile acuity of that area.

6.1.5 Encoding Jitter

In our default model, for each participant, the RF grid was shifted by a value drawn from a uniform distribution (Eq. 2.1.1). The maximum value for deviation was half of RF center-to-center spacing. The purpose of this phase shift from one participant to the next was to prevent idiosyncrasies that could arise from stimuli landing on the RF centers. Nevertheless, our default skin patch is an idealized model. Although our model takes into account two sources of cortical noise, spontaneous activity and Poisson firing rate variability, it is still idealized with respect to the position and characteristics of RFs. To explore how our Bayesian observer would perform with these additional sources of encoding noise, we jittered the individual RFs' position, sigma, and amplitude based on Eq. 2.1.2. Our Bayesian observer performed relatively well when J = 2, despite its state of awareness of the noise **(Fig. 3.7A)**. However, at J = 5, the performance of the Bayesian observer that was unaware of the jitters was considerably impacted across all 2PD tasks. Still, the Bayesian observer was quite robust to this noise. Yet again, the performance of S2PD was greater than the other tasks, and the decrease in the performance due to noise was less than the others. Interestingly, when the Bayesian observer was aware of all the jitters, the performance was better than the no-jitter condition at early separation distances,

suggesting that the variable RFs are more informative than uniform RFs. The total number of spike counts in the jitter condition was also higher than in the no-jitter condition, further explaining the increase in performance in the jitter-aware condition. When we looked at how jitter awareness regarding individual RF characteristics affected the performance, we found that awareness regarding the RF amplitude made the least difference in performance. Awareness regarding the position of RF centers resulted in the most difference in the performance of tasks, suggesting that position awareness is the most informative RF characteristic for the Bayesian observer. Some investigators have argued that the brain receives detailed stimulus information such as signalled edge orientation (Pruszynski & Johansson, 2014) from peripheral afferents. Our results suggest if the brain is Bayesian then it does not necessarily need to receive detailed information regarding its RF property and the stimulus to perform relatively well on acuity tasks.

6.1.6 Stimulus Probe Size

For the sake of simplicity, the stimuli in our default model are points with no width. In reality, stimuli used in 2PD tasks have width and surface area. For example, Mancini et al. (2014) used a 0.2 mm Frey filaments to map tactile acuity across body. The fact that stimuli have width means that there is a practical limit to a separation distance that an experimenter could test when using a two-point stimulus. In the case of Mancini et al. (2014) study, that limit would be 0.4 mm. This limitation does not apply to S2PD because only one stimulus point is delivered at any given time. To test the effect of radial stimuli on performance, we came up with two experimental paradigms, the variable-indentation and the fixed-indentation. In the

variable indentation paradigm, the intensity of stimuli was adjusted such that the total spike count would remain the same regardless of stimulus surface area. In the fixed indentation paradigm, the total spike count is not controlled; meaning, the larger the stimulus radius, the higher the total spike count. We found that stimulus radius was inversely correlated with performance under the variable-indentation paradigm, suggesting that a smaller stimulus with higher intensity is more informative to the Bayesian observer than a larger stimulus with smaller intensity. When we do not control for the spike count in the fixed-indentation paradigm, the larger the stimulus radius the higher the performance in S2PD. This increase in performance can be explained as a larger stimulus radius results in a higher total spike count. However, the stimulus radius does not significantly impact the performance in C2PD and 2POD, indicating that the benefit of a higher spike count is offset by a rise in ambiguity in inferring two-point stimulus separation.

6.2 Character Recognition Tasks

Character recognition tasks are another method of assessing tactile spatial acuity. The benefit of this method is that because it involves many point stimuli, the effect of the magnitude cue would be minimized (Johansson et al., 1980). Furthermore, this task is suggested as a convenient alternative to the 2PD tasks as it does not require participant training and careful calliper manipulation. Bruns et al. (2014) came up with a tactile acuity chart similar to a Snellen eye chart in which they used Braille characters of various sizes and orientations as stimuli. The threshold of participants on this task was similar to C2PD threshold (Bruns et al., 2014). We simulated two variations of this task, raised letter and Braille character recognition, under a

force-control paradigm. For both tasks, we looked at the effect of moving stimulus presentation (movement) and static stimulus presentation (static). We found that repeated static touch had a similar performance to movement touch. However, movement touch had a higher average hit rate than static touch, similar to the findings in humans (M. Heller, 1986; Loomis, 1974). In movement and repeated static touch, the Bayesian observer receives more information regarding the stimulus through multiple sampling, resulting in increased performance.

In RLRT, embossed letters are often used as stimuli (Johnson & Phillips, 1981b; Loomis, 1982). However, for our simulation, we represented upper case English alphabet letters as a set of points (dotted letters) in a similar manner to those produced by Optacon (Efron, 1977). Human participants' performance with dotted letters is similar to their performance with embossed letters with a thin font but better than embossed letters with a bolded font (Geyer & Gupta, 1981; Loomis, 1981). By adjusting the stimulus intensity of in our simulations, we fitted the Bayesian observer's average hit rate to that of human participants (Craig, 1979). The resulting confusion matrix showed considerable similarity to the human confusion matrix. Similar to the human participants, on average the Bayesian observer responded correctly to all letter stimuli. Among the top ten incorrect responses, there were some similarities between the model and humans, such as confusing letters $Q\&O$, $P\&\mathrm{F}$ and $M\&W$. We also looked at whether letter similarity predict performance on RLRT. We found that letter similarity was moderately correlated with the Bayesian observer's incorrect stimulus-response pair and weakly correlated with the human participant's incorrect stimulus-response pair.

In the visual psychophysics literature, masking refers to the interference of one

stimulus with the recognition of another stimulus (target). In particular, lateral masking, which is the interference of a masking stimulus in recognition of an adjacent letter, has been extensively studied in linguistic literature. In studies of visual letter recognition tasks, lateral masking has been shown to decrease the perceptibility of letters (Massaro & Klitzke, 1979), such that the closer the masking stimulus to the target letter, the smaller the performance(Huckauf & Heller, 2002; Huckauf et al., 1999; Nazir, 1992). Similarly, lateral masking has been shown to decrease the performance in RLRT based on the proximity of the masking stimulus to the target letter (Loomis & Apkarian-Stielau, 1976). To explore the effect of masking in RLRT, we flanked stimulus letters with masking columns. Our results concur with the findings in the literature. The Bayesian observer performed worse the closer the masking stimuli were to the stimulus letter. Additionally, we predicted that masking unawareness lowers the performance in RLRT. Masking stimuli lower performance by introducing a new source of noise to the model. Even when the Bayesian observer is aware of masking stimuli, it still performs worse than the no-masking condition because the added action potentials increase the ambiguity of letters and makes it harder to infer what the true stimulus letter was.

Similar to the RLRT, we fitted the Bayesian observer's average hit rate on the BCRT to the average hit rate of human participants (Craig, 1979). The resulting confusion matrix was highly correlated with the human confusion matrix. We also simulated BCRT under displacement control. The average hit rate was higher under displacement-control compared to the force-control. However, when the average hit rate was fit to human data, the resulting matrix was highly correlated with the human and simulated force-control confusion matrices. Yet, there were quite a few

letter outliers between the two paradigms. For example, the performance of the Bayesian observer on Braille characters Q (⠟), G(⠛), and Y(⠽) was higher in the displacement-control paradigm than in the force-control, and the performance of Braille characters A (⠁), B(⠃), and C(⠉) was higher in the force-control than in the displacement-control. This pattern is expected as Braille characters with a high number of dots (i.e., Q, G, Y) have higher total spike counts under the displacement-control paradigm, and Braille characters with a low number of dots (i.e., A, B, C) have higher point intensity under the force-control paradigm, making them more distinguishable.

The Snellen chart is based on the principle that the size of a letter corresponds to recognition difficulty. Similarly, the larger the size of a Braille character is, the higher the recognition accuracy (Loomis, 1981). The height of Braille dots is shown to be correlated with reading speed (Lei et al., 2019) and performance (Douglas et al., 2009). Similarly, we found that changing character scale and stimulus intensity increases the average hit rate. The performance was higher under displacement control than under force-control. Our result suggests that Braille can be made easier by increasing the size of the characters and increasing the height of the dots; nevertheless, larger Braille characters can make the overall readability lower by reducing the number of characters that can be put in a line.

6.3 Illusions

6.3.1 Orientation Anisotropy Illusion

Longo and Haggard (2011) discovered an illusion in which stimulus separations on the dorsum are perceived larger when oriented transversely than longitudinally. For the sake of convenience, we call this illusion orientation anisotropy illusion. The authors suggested that this illusion arises from a distorted representation of the hand shape in the brain. In other words, there is a mismatch between the generative stage of the encoder and that assumed by the decoder. To explore what could underlie this mismatch, we investigated how the RFs in the dorsum of the hand differed from the RFs in the palm.

Studies of tactile acuity have reported that the measured thresholds are dependent on the orientation of the stimulus (Essock et al., 1992; G. O. Gibson & Craig, 2005; Stevens & Patterson, 1995). In fact, Weber was the first to report that the two-point discrimination threshold was smaller when the stimulus was orientated transversely rather than longitudinally (Weber et al., 2018). Studies of peripheral afferents found that 50% of the RFs are elongated longitudinally (Bensmaïa et al., 2006; Johansson & Vallbo, 1980; Knibestöl & Vallbo, 1970). Brown et al. (1975) demonstrated that in the elongated RFs, their long axis may be more than twice as long as the short axis on the hairy skins. RF elongation is also accompanied by closer RF spacing (G. O. Gibson & Craig, 2006); meaning, the RF centers are closer together in the transverse direction than the longitudinal direction. Not only the RFs of peripheral afferents are elliptical but the RFs of cortical neurons are elliptical as well. In adult owl and squirrel monkeys, neurons in SI whose RFs are located on the hand are shown to

be elongated longitudinally (Jenkins et al., 1990; Merzenich et al., 1983; Merzenich et al., 1984; Sur et al., 1982). To measure RF shape anisotropy, we extracted RF dimensions and spacing from Merzenich et al. (1987) which extensively mapped and recorded from neurons in cortical areas 3b and 1 (Fig .5.2). We noticed that on average the RFs on the dorsum of the hand are more elliptical than the ones in the palm of the hand, and the RF spacing in the dorsum of the hand is smaller in the transverse direction than in the longitudinal direction.

By updating our model parameters according to our findings from Merzenich et al. (1987), we were able to replicate the illusion under an unaware condition. When our Bayesian observer was aware of the RFs shape and spacing anisotropy, only a slight shift in the psychometric curves was observed. However, when the Bayesian observer assumed that the RFs are circular and equidistant from their neighbours, a significant shift in the psychometric curves were observed. We observed this shift in both sides of the hand with the dorsum showing a greater shift. Several investigators have reported no OAI on the palm of the hand (Cholewiak, 1999; Green, 1982; Longo & Haggard, 2011); however, recent studies have demonstrated a significant but smaller in magnitude anisotropy on the palm of the hand (Fiori & Longo, 2018; Knight et al., 2014; Longo et al., 2015).

The anisotropy in the spacing and sigma of the RFs means that separation distances are perceived differently depending on whether the orientation of the stimuli is longitudinal or transverse. Consequently one would expect that perception of separation distances of stimuli that are oriented obliquely ($\pm 45°$) would not be different. Because all the RFs spacing and shapes are elongated longitudinally, the perception of oblique stimuli of either $+45°$ or $-45°$ from the longitudinal axis is affected to

the same degree, so we would not expect a bias in either oblique direction. Indeed, our simulation of the OAI experiment using oblique stimuli showed no occurrence of illusion, regardless of RF shape anisotropy awareness. However, unawareness resulted in shallower curves, which stems from the decoder's inaccurate understanding of the generative stage. Furthermore, the psychometric curves for the palm of the hand were shallower than the curves for the dorsum, which can be explained as the RF density in the transverse direction at the dorsum of the hand is greater than the palm of the hand, and the RF area in the dorsum is smaller than the palm.

We also explored how awareness regarding different sigma and spacing ratios affects PSE. In general, when the Bayesian observer is aware of its RF characteristics such as sigma and spacing ratio, we do not observe a significant change in the PSE. However, when the Bayesian observer is not aware of its RF characteristics, we see a noticeable shift in PSE at certain sigma and spacing ratios. For example, we predict that if an area of skin has a sigma and spacing ratio of 1.8 then we would expect objects to be perceived as smaller when oriented transversely than longitudinally, opposite to the OAI.

6.3.2 Adaptation Induced Repulsion Illusion

Studies of visual adaptation have given us insight into mechanisms underlying vision. A notable example of visual adaptation is the tilt aftereffect illusion. In this illusion, adaptation to a stimulus line causes subsequent line stimuli to be perceived titled away from the adapted orientation (J. J. Gibson & Radner, 1937). Schwartz et al. (2007) proposes that illusions such as the tilt aftereffect could arise from downstream

decoders not being aware of the tuning changes brought on by contextual cues. Inspired by the aftereffect illusion, Li et al. (2017) demonstrated an adaptation-induced repulsion illusion in the sense of touch. Li et al. (2017) proposed that a Bayesian observer could replicate this illusion if it does not take the adaption of the state of the sensory neurons into account when decoding. To test this proposal, we simulated AIRI with a focal adaptation at the center of our skin patch. When the Bayesian observer was aware of the adaptation state of its neurons, the performance did not differ greatly between the adapted and unadapted conditions. The slope of the psychometric curve decreased slightly in the adapted condition because adaptation decreases the signal-to-noise ratio. However, when the Bayesian observer was unaware of the adaptation state of its neurons, the psychometric curve for the adapted condition shifted to the right, meaning, stimulus separations were perceived to be larger than what they really were. Increasing the adaptation level resulted in a higher shift of psychometric function under the unaware-adapted condition, meaning, the strength of the illusion could be enhanced by either increasing the adapting stimulus frequency or prolonging the duration of adaptation. Based on the result of our simulation, we predicted that if two focal adaptors were placed at the flanks of a two-point stimulus then stimulus separation distance would feel smaller than it really was. Similar to the default AIRI, increasing the adaptation level strengthens the illusion.

6.4 Noise and Uncertainty

The variable response seen in human participants across many different psychophysical studies suggests underlying mechanisms that are prone to randomness. Although the source of this trial-to-trial variability is not fully understood, the noise observed

in the cortical neurons presumably is the result of the accumulation of noise through the sensory transduction and transmission pathway. According to the theory of information processing inequality, the information content of a signal cannot be increased in the subsequent steps of operation (Latham & Roudi, 2009). Therefore, a cortical decoder is not able to perform better than a hypothetical decoder that has access to peripheral sensory information. Each step of the sensory transmission pathway introduces a degree of uncertainty. When a stimulus touches our skin, the skin dynamic ever so slightly varies, causing the discharge of the mechanoreceptors to vary as well. Along the sensory transmission pathway, there are many sources of stochastic noise such as the opening and closing of ion channels (Kispersky & White, 2008), vesicle diffusion (Lou et al., 2005), and the binding of neurotransmitters (Maio et al., 2017). Yet, surprisingly little noise can be seen in the recordings of afferents, suggesting that the majority of noise inherent in perception originates in the cortex (Hay & Pruszynski, 2020). Not every neuron in the cortex exhibits the same level of neuronal variability. Many cortical neurons fire in a highly variable manner resembling Poisson (Moreno-Bote, 2014; Shadlen & Newsome, 1998; Tomko & Crapper, 1974) or Gamma (Tomko & Crapper, 1974) distributions, whereas others have less variable responses (DeWeese et al., 2003; Gur et al., 1997). A neuron can also have a different response variability depending on the stimulus (Warzecha & Egelhaaf, 1999). A growing viewpoint suggests that the noise observed in the nervous system may have computational benefits.

6.4.1 Purpose of Noise

Some studies have shown that the stochasticity in neuronal response is tightly controlled and regulated by neuronal machinery, suggesting that the noise observed in neurons may serve valuable functions. Several computational approaches have adopted noise to improve processing information. Benzi et al. (1981) proposed a process termed stochastic resonance by which the sensitivity of a system to weak signals can be enhanced at certain noise intensity. Synaptic noise has been shown to increase the probability of response to a weak signal in pyramidal cells (Shu et al., 2003). In crayfish mechanoreceptors, the addition of an intermediate level of external noise enhanced signal transmission; however, the addition of a high level of noise degraded signal transmission (Douglass et al., 1993). Similarly, external noise was shown to enhance SA1 afferent response to a weak signal (Collins et al., 1996). A variation of this mechanism, inverse stochastic resonance, by which noise of particular intensity reduces the excitability of neurons (Uzuntarla et al., 2017) has been observed in Purkinje cells (Buchin et al., 2016). Thus, a certain level of noise can increase the probability that sub-threshold signals reach the threshold. However, high levels of noise can render supra-threshold signals meaningless. The addition of noise to neural network models has been demonstrated to make the models more robust, increase model generalizability (reducing over-fitting), and facilitate learning (Kirkpatrick et al., 1983; Krogh & Hertz, 1992). Similarly, the brain may be generating noise to enhance learning.

6.4.2 Managing Noise

As mentioned, the noise in a system can not be diminished in subsequent processing (Latham & Roudi, 2009); however, the brain may employ strategies to mitigate the negative consequences of noise while still benefiting from its computational advantages. Two of these strategies are by averaging signals and using prior knowledge. Averaging may be applied when there is a redundancy of information such as when multiple neurons carry the same signals with independent sources of noise (Ferster, 1996). Additionally, prior knowledge can be used to help reduce noise. When the expected statistical structure of a stimulus is known, the signal can be distinguished from the noise (Turin, 1960). These two strategies are embedded in the Bayesian inference framework. A Bayesian observer uses prior knowledge and noisy observations to calculate the probabilities of hypotheses about the state of the world. We have shown that increasing the duplication factor increases the performance of the model, which is similar to reducing noise through averaging. Furthermore, when the Bayesian observer was aware of the encoding jitter, it was also able to perform better than when it did not know the detailed structure of its encoding stage. In this thesis, we have shown that the Bayesian observer is capable of replicating general trends in the tactile spatial literature, and it can be used to make sense of data and predict behaviour.

Appendix A

Values Used

Table A.1: Values used for the simulation.

Variable	**Value**	**Citation**
Spontaneous Firing Rate ($r_{spontaneous}$)	$10\,AP/s$	Vazquez et al. (2013)
Response Rate	$r_{ON} = 62\,AP/s$ $r_{SUSTAIN} = 8\,AP/s$ $r_{OFF} = 43\,AP/s$	Pei et al. (2009)
Stimulation Duration	$t_{ON} = 0.04s$ $t_{SUSTAIN} = 0.42s$ $t_{OFF} = 0.04s$	Pei et al. (2009)
Sigma (σ)	forearm: $15\,mm$ fingertip: $2\,mm$	Sur et al. (1980)
Adaptor Radius	$9.5\,mm$	Li et al. (2017)
Spacing Between RF Centers	$15\,mm$	Arbitrarily decided
Skin Dimension	$150\,mm \times 150\,mm$	Arbitrarily decided
Number of Participants	150	Arbitrarily decided
Number of Trails Per Participants	150	Arbitrarily decided

Bibliography

Alloway, K. D., Rosenthal, P., & Burton, H. (1989). Quantitative measurements of receptive field changes during antagonism of GABAergic transmission in primary somatosensory cortex of cats. *Experimental Brain Research*, *78*(3), 514–532. https://doi.org/10.1007/BF00230239

Arielle Michal Silverman, P. D., & Edward C. Bell, P. D. (2018). The association between braille reading history and well-being for blind adults abstract. Retrieved November 15, 2022, from https://nfb.org/images/nfb/publications/jbir/jbir18/jbir080103.html

Bensmaïa, S. J., Craig, J. C., Yoshioka, T., & Johnson, K. O. (2006). SA1 and RA afferent responses to static and vibrating gratings. *Journal of neurophysiology*, *95*(3), 1771–1782. https://doi.org/10.1152/jn.00877.2005

Benzi, R., Sutera, A., & Vulpiani, A. (1981). The mechanism of stochastic resonance. *Journal of Physics A: Mathematical and General*, *14*(11), L453–L457. https://doi.org/10.1088/0305-4470/14/11/006

Breitmeyer, B., & Ogmen, H. (2006, April). *Visual masking: Time slices through conscious and unconscious vision*. Oxford University Press. https://doi.org/10.1093/acprof:oso/9780198530671.001.0001

Brown, P. B., Fuchs, J. L., & Tapper, D. N. (1975). Parametric studies of dorsal horn neurons responding to tactile stimulation. *Journal of Neurophysiology*, *38*(1), 19–25. https://doi.org/10.1152/jn.1975.38.1.19

Bruns, P., Camargo, C. J., Campanella, H., Esteve, J., Dinse, H. R., & Röder, B. (2014). Tactile acuity charts: A reliable measure of spatial acuity. *PLoS ONE*, *9*(2), e87384. https://doi.org/10.1371/journal.pone.0087384

Buchin, A., Rieubland, S., Häusser, M., Gutkin, B. S., & Roth, A. (2016). Inverse stochastic resonance in cerebellar purkinje cells. *PLoS Computational Biology*, *12*(8). https://doi.org/10.1371/journal.pcbi.1005000

Cholewiak, R. W. (1999). The perception of tactile distance: Influences of body site, space, and time [Publisher: SAGE Publications Ltd STM]. *Perception*, *28*(7), 851–875. https://doi.org/10.1068/p2873

Collins, J. J., Imhoff, T. T., & Grigg, P. (1996). Noise-enhanced information transmission in rat SA1 cutaneous mechanoreceptors via aperiodic stochastic resonance [Publisher: American Physiological Society]. *Journal of Neurophysiology*, *76*(1), 642–645. https://doi.org/10.1152/jn.1996.76.1.642

Colman, A. M. (2009). A dictionary of psychology [Edition: 3rd ed. ISBN: 9780191726828 Place: Oxford].

Craig, J. C. (1976). Vibrotactile letter recognition: The effects of a ma king stimulus. *Perception & Psychophysics*, *20*(5), 317–326. https://doi.org/10.3758/BF03199412

Craig, J. C. (1979). A confusion matrix for tactually presented letters. *Perception & Psychophysics*, *26*(5), 409–411. https://doi.org/10.3758/BF03204167

Craig, J. C., & Johnson, K. O. (2000). The two-point threshold: Not a measure of tactile spatial resolution [Publisher: SAGE Publications Inc]. *Current Directions in Psychological Science*, *9*(1), 29–32. https://doi.org/10.1111/1467-8721.00054

Craig, J. C., & Lyle, K. B. (2001). A comparison of tactile spatial sensitivity on the palm and fingerpad. *Perception & Psychophysics*, *63*(2), 337–347. https://doi.org/10.3758/BF03194474

Daroff, R., & Aminoff, M. (2014). *Encyclopedia of the neurological sciences*. Elsevier Science. https://books.google.ca/books?id=hfjSVIWViRUC

Davidson, P. W., Wiles-Kettenmann, M., Haber, R. N., & Appelle, S. (1980). Relationship between hand movements, reading competence and passage difficulty in braille reading. *Neuropsychologia*, *18*(6), 629–635. https://doi.org/10.1016/0028-3932(80)90102-5

Day, R. H., & Singer, G. (1964). A tactile spatial aftereffect [Publisher: Routledge _eprint: https://doi.org/10.1080/00049536408255500]. *Australian Journal of Psychology*, *16*(1), 33–37. https://doi.org/10.1080/00049536408255500

Dayan, P., & Abbott, L. F. (2001). *Theoretical neuroscience: Computational and mathematical modeling of neural systems*. Massachusetts Institute of Technology Press.

DeWeese, M. R., Wehr, M., & Zador, A. M. (2003). Binary spiking in auditory cortex [Publisher: Society for Neuroscience Section: Behavioral/Systems/Cognitive]. *Journal of Neuroscience*, *23*(21), 7940–7949. https://doi.org/10.1523/JNEUROSCI.23-21-07940.2003

Doetsch, G. S., Stoney, S. D., & Hauge, D. H. (1992). Convergent inputs to single neurons in two different subdivisions of somatosensory forepaw digit cortex of the raccoon. *Experimental Neurology*, *115*(2), 250–259. https://doi.org/10.1016/0014-4886(92)90059-Y

Douglas, G., Weston, A., Whittaker, J., Wilkins, S. M., & Robinson, D. (2009). An investigation of the height of embossed braille dots for labels on pharmaceutical products [Publisher: SAGE Publications Inc]. *Journal of Visual Impairment & Blindness*, *103*(10), 662–667. https://doi.org/10.1177/0145482X0910301009

Douglass, J. K., Wilkens, L., Pantazelou, E., & Moss, F. (1993). Noise enhancement of information transfer in crayfish mechanoreceptors by stochastic resonance [Number: 6444 Publisher: Nature Publishing Group]. *Nature*, *365*(6444), 337–340. https://doi.org/10.1038/365337a0

Efron, N. (1977). Optacon—a replacement for braille?* [_eprint: https://onlinelibrary.wiley.com/doi/0938.1977.tb02825.x]. *The Australian Journal of Optometry*, *60*(4), 118–129. https://doi.org/10.1111/j.1444-0938.1977.tb02825.x

Essick, G. K., Chen, C. C., & Kelly, D. G. (1999). A letter-recognition task to assess lingual tactile acuity. *Journal of Oral and Maxillofacial Surgery*, *57*(11), 1324–1330. https://doi.org/10.1016/S0278-2391(99)90871-6

Essock, E. A., Krebs, W. K., & Prather, J. R. (1992). An anisotropy of human tactile sensitivity and its relation to the visual oblique effect. *Experimental Brain Research*, *91*(3), 520–524. https://doi.org/10.1007/BF00227848

Ferster, D. (1996). Is neural noise just a nuisance? [Publisher: American Association for the Advancement of Science]. *Science*, *273*(5283), 1812–1813. Retrieved October 27, 2022, from http://go.gale.com/ps/i.do?p=AONE&sw=w&issn=

00368075&v=2.1&it=r&id=GALE%7CA18748040&sid=googleScholar&linkaccess=abs

Fiori, F., & Longo, M. R. (2018). Tactile distance illusions reflect a coherent stretch of tactile space. *Proceedings of the National Academy of Sciences*, *115*(6), 1238–1243. https://doi.org/10.1073/pnas.1715123115

Geisler, W. S., & Kersten, D. (2002). Illusions, perception and bayes [Bandiera_abtest: a Cg_type: Nature Research Journals Number: 6 Primary_atype: News & Views Publisher: Nature Publishing Group]. *Nature Neuroscience*, *5*(6), 508–510. https://doi.org/10.1038/nn0602-508

Geyer, L. H., & Gupta, S. M. (1981). Recognition/confusion of dot matrix vs. conventional font capital letters [Place: US Publisher: Psychonomic Society]. *Perception & Psychophysics*, *29*, 280–282. https://doi.org/10.3758/BF03207295

Gibson, G. O., & Craig, J. C. (2005). Tactile spatial sensitivity and anisotropy. *Perception & Psychophysics*, *67*(6), 1061–1079. https://doi.org/10.3758/BF03193632

Gibson, G. O., & Craig, J. C. (2006). The effect of force and conformance on tactile intensive and spatial sensitivity. *Experimental Brain Research*, *170*(2), 172–181. https://doi.org/10.1007/s00221-005-0200-1

Gibson, J. J., & Radner, M. (1937). Adaptation, after-effect and contrast in the perception of tilted lines. i. quantitative studies [Num Pages: 453-467 Place: Washington, US Publisher: Psychological Review Company (US)]. *Journal of Experimental Psychology*, *20*(5), 453–467. https://doi.org/10.1037/h0059826

Gilbert, C. D., & Wiesel, T. N. (1992). Receptive field dynamics in adult primary visual cortex [Number: 6365 Publisher: Nature Publishing Group]. *Nature*, *356*(6365), 150–152. https://doi.org/10.1038/356150a0

Goldreich, D. (2007). A bayesian perceptual model replicates the cutaneous rabbit and other tactile spatiotemporal illusions [Publisher: Public Library of Science]. *PLOS ONE*, *2*(3), e333. https://doi.org/10.1371/journal.pone.0000333

Goldreich, D., & Tong, J. (2013). Prediction, postdiction, and perceptual length contraction: A bayesian low-speed prior captures the cutaneous rabbit and related illusions. *Frontiers in Psychology*, *4*. Retrieved November 6, 2022, from https://www.frontiersin.org/articles/10.3389/fpsyg.2013.00221

Green, B. G. (1982). The perception of distance and location for dual tactile pressures. *Perception & Psychophysics*, *31*(4), 315–323. https://doi.org/10.3758/BF03202654

Gur, M., Beylin, A., & Snodderly, D. M. (1997). Response variability of neurons in primary visual cortex (v1) of alert monkeys [Publisher: Society for Neuroscience Section: Articles]. *Journal of Neuroscience*, *17*(8), 2914–2920. https://doi.org/10.1523/JNEUROSCI.17-08-02914.1997

Hay, E., & Pruszynski, J. A. (2020). Orientation processing by synaptic integration across first-order tactile neurons [Publisher: Public Library of Science]. *PLOS Computational Biology*, *16*(12), e1008303. https://doi.org/10.1371/journal.pcbi.1008303

Helen, E. R., David, J. M., Ross, H. E., & Murray, D. J. (Eds.). (2018, October 24). *E.h. weber on the tactile senses* (2nd ed.). Psychology Press. https://doi.org/10.4324/9781315782089

Heller, M. (1986). Active and passive tactile braille recognition. *Bulletin of the Psychonomic Society*, *24*, 201–202. https://doi.org/10.3758/BF03330548

Heller, M. (1993). Influence of visual guidance on braille recognition: Low lighting also helps touch. *Perception & Psychophysics*, *54*, 675–681. https://doi.org/10.3758/BF03211791

Hoskin, E. R., Coyne, M. K., White, M. J., Dobri, S. C. D., Davies, T. C., & Pinder, S. D. (2022). Effectiveness of technology for braille literacy education for children: A systematic review. *Disability and Rehabilitation: Assistive Technology*, 1–11. https://doi.org/10.1080/17483107.2022.2070676

Huckauf, A., & Heller, D. (2002). What various kinds of errors tell us about lateral masking effects [Publisher: Routledge _eprint: https://doi.org/10.1080/13506280143000548A] *Visual Cognition*, *9*(7), 889–910. https://doi.org/10.1080/13506280143000548A

Huckauf, A., Heller, D., & Nazir, T. A. (1999). Lateral masking: Limitations of the feature interaction account. *Perception & Psychophysics*, *61*(1), 177–189. https://doi.org/10.3758/BF03211958

Jenkins, W. M., Merzenich, M. M., Ochs, M. T., Allard, T., & Guic-Robles, E. (1990). Functional reorganization of primary somatosensory cortex in adult owl monkeys after behaviorally controlled tactile stimulation [Publisher: American Physiological Society]. *Journal of Neurophysiology*, *63*(1), 82–104. https://doi.org/10.1152/jn.1990.63.1.82

Johansson, R. S., & Vallbo, Å. B. (1980). Spatial properties of the population of mechanoreceptive units in the glabrous skin of the human hand. *Brain Research*, *184*(2), 353–366. https://doi.org/10.1016/0006-8993(80)90804-5

Johansson, R. S., Vallbo, Å. B., & Westling, G. (1980). Thresholds of mechanosensitive afferents in the human hand as measured with von frey hairs. *Brain Research*, *184*(2), 343–351. https://doi.org/10.1016/0006-8993(80)90803-3

Johnson, K. O., & Phillips, J. R. (1981a). Tactile spatial resolution. i. two-point discrimination, gap detection, grating resolution, and letter recognition [Publisher: American Physiological Society]. *Journal of Neurophysiology*, *46*(6), 1177–1192. https://doi.org/10.1152/jn.1981.46.6.1177

Johnson, K. O., & Phillips, J. R. (1981b). Tactile spatial resolution. i. two-point discrimination, gap detection, grating resolution, and letter recognition [Publisher: American Physiological Society]. *Journal of Neurophysiology*, *46*(6), 1177–1192. https://doi.org/10.1152/jn.1981.46.6.1177

Johnson, K. O., & Phillips, J. R. (1981c). Tactile spatial resolution. i. two-point discrimination, gap detection, grating resolution, and letter recognition. *Journal of Neurophysiology*, *46*(6), 1177–1192. https://doi.org/10.1152/jn.1981.46.6.1177

Johnson, K. O., Yoshioka, T., & Vega–Bermudez, F. (2000). Tactile functions of mechanoreceptive afferents innervating the hand. *Journal of Clinical Neurophysiology*, *17*(6), 539–558. Retrieved October 21, 2022, from http://journals.lww.com/clinicalneurophys/Fulltext/2000/11000/Tactile_Functions_of_Mechanoreceptive_Afferents.2.aspx

Jones, L. A., & Smith, A. M. (2014). Tactile sensory system: Encoding from the periphery to the cortex [_eprint: https://onlinelibrary.wiley.com/doi/pdf/10.1002/wsbm.1267]. *WIREs Systems Biology and Medicine*, *6*(3), 279–287. https://doi.org/https://doi.org/10.1002/wsbm.1267

Kaas, J. H., Merzenich, M. M., & Killackey, H. P. (1983). The reorganization of somatosensory cortex following peripheral nerve damage in adult and developing mammals [_eprint: https://doi.org/10.1146/annurev.ne.06.030183.001545]. *Annual Review of Neuroscience*, *6*(1), 325–356. https://doi.org/10.1146/annurev.ne.06.030183.001545

Kang, R., Herman, D., MacGillis, M., & Zarzecki, P. (1985). Convergence of sensory inputs in somatosensory cortex: Interactions from separate afferent sources. *Experimental Brain Research*, *57*(2), 271–278. https://doi.org/10.1007/BF00236532

Kirkpatrick, S., Gelatt, C. D., & Vecchi, M. P. (1983). Optimization by simulated annealing [Publisher: American Association for the Advancement of Science]. *Science*, *220*(4598), 671–680. https://doi.org/10.1126/science.220.4598.671

Kispersky, T., & White, J. A. (2008). Stochastic models of ion channel gating. *Scholarpedia*, *3*(1), 1327. https://doi.org/10.4249/scholarpedia.1327

Knibestöl, M., & Vallbo, Å. B. (1970). Single unit analysis of mechanoreceptor activity from the human glabrous skin [_eprint: https://onlinelibrary.wiley.com/doi/pdf/10.1111/j.1748-1716.1970.tb04783.x]. *Acta Physiologica Scandinavica*, *80*(2), 178–195. https://doi.org/10.1111/j.1748-1716.1970.tb04783.x

Knight, F. L. C., Longo, M. R., & Bremner, A. J. (2014). Categorical perception of tactile distance. *Cognition*, *131*(2), 254–262. https://doi.org/10.1016/j.cognition.2014.01.005

Kontsevich, L. L., & Tyler, C. W. (1999). Bayesian adaptive estimation of psychometric slope and threshold. *Vision Research*, *39*(16), 2729–2737. https://doi.org/10.1016/s0042-6989(98)00285-5

Krogh, A., & Hertz, J. A. (1992). Generalization in a linear perceptron in the presence of noise. *Journal of Physics A: Mathematical and General*, *25*(5), 1135. https://doi.org/10.1088/0305-4470/25/5/020

Latham, P. E., & Roudi, Y. (2009). Mutual information. *Scholarpedia*, *4*(1), 1658. https://doi.org/10.4249/scholarpedia.1658

Lei, D., Stepien-Bernabe, N. N., Morash, V. S., & MacKeben, M. (2019). Effect of modulating braille dot height on reading regressions. *PloS One*, *14*(4), e0214799. https://doi.org/10.1371/journal.pone.0214799

Li, L., Chan, A., Iqbal, S. M., & Goldreich, D. (2017). An adaptation-induced repulsion illusion in tactile spatial perception. *Frontiers in Human Neuroscience*, *11*, 331. https://doi.org/10.3389/fnhum.2017.00331

Longo, M. R., Ghosh, A., & Yahya, T. (2015). Bilateral symmetry of distortions of tactile size perception [Publisher: SAGE Publications Ltd STM]. *Perception*, *44*(11), 1251–1262. https://doi.org/10.1177/0301006615594949

Longo, M. R., & Haggard, P. (2011). Weber's illusion and body shape: Anisotropy of tactile size perception on the hand [Num Pages: 720-726 Place: Washington, US Publisher: American Psychological Association (US)]. *Journal of Experimental Psychology: Human Perception and Performance*, *37*(3), 720–726. https://doi.org/http://dx.doi.org.libaccess.lib.mcmaster.ca/10.1037/a0021921

Loomis, J. M. (1974). Tactile letter recognition under different modes of stimulus presentation. *Perception & Psychophysics*, *16*(2), 401–408. https://doi.org/10.3758/BF03203960

Loomis, J. M. (1981). On the tangibility of letters and braille. *Perception & Psychophysics*, *29*(1), 37–46. https://doi.org/10.3758/BF03198838

Loomis, J. M. (1982). Analysis of tactile and visual confusion matrices. *Perception & Psychophysics*, *31*(1), 41–52. https://doi.org/10.3758/BF03206199

Loomis, J. M., & Apkarian-Stielau, P. (1976). A lateral masking effect in tactile and blurred visual letter recognition. *Perception & Psychophysics*, *20*(4), 221–226. https://doi.org/10.3758/BF03199447

Lou, X., Scheuss, V., & Schneggenburger, R. (2005). Allosteric modulation of the presynaptic ca2+ sensor for vesicle fusion [Number: 7041 Publisher: Nature Publishing Group]. *Nature*, *435*(7041), 497–501. https://doi.org/10.1038/nature03568

Lundborg, G., & Rosén, B. (2004). The two-point discrimination test – time for a re-appraisal? *The Journal of Hand Surgery: British & European Volume*, *29*(5), 418–422. https://doi.org/10.1016/j.jhsb.2004.02.008

Ma, W. J., Beck, J. M., Latham, P. E., & Pouget, A. (2006). Bayesian inference with probabilistic population codes [Bandiera_abtest: a Cg_type: Nature Research Journals Number: 11 Primary_atype: Research Publisher: Nature Publishing Group]. *Nature Neuroscience*, *9*(11), 1432–1438. https://doi.org/10.1038/nn1790

Macgillis, M., Kang, R., Herman, D., & Zarzecki, P. (1983). Interactions among convergent inputs to somatosensory cortex neurons. *Brain Research*, *276*(2), 329–332. https://doi.org/10.1016/0006-8993(83)90741-2

Maio, V. D., Ventriglia, F., & Santillo, S. (2017). Stochastic, structural and functional factors influencing AMPA and NMDA synaptic response variability: A review [Publisher: Portland Press]. *Neuronal Signaling*, *1*(3). https://doi.org/10.1042/NS20160051

Mancini, F., Bauleo, A., Cole, J., Lui, F., Porro, C. A., Haggard, P., & Iannetti, G. D. (2014). Whole-body mapping of spatial acuity for pain and touch. *Annals of Neurology*, *75*(6), 917–924. https://doi.org/10.1002/ana.24179

Maricich, S. M., Wellnitz, S. A., Nelson, A. M., Lesniak, D. R., Gerling, G. J., Lumpkin, E. A., & Zoghbi, H. Y. (2009). Merkel cells are essential for light touch responses. *Science (New York, N.Y.)*, *324*(5934), 1580–1582. https://doi.org/10.1126/science.1172890

Massaro, D. W., & Klitzke, D. (1979). The role of lateral masking and orthographic structure in letter and word recognition. *Acta Psychologica*, *43*(5), 413–426. https://doi.org/10.1016/0001-6918(79)90033-7

Merzenich, M. M., Kaas, J. H., Wall, J., Nelson, R. J., Sur, M., & Felleman, D. (1983). Topographic reorganization of somatosensory cortical areas 3b and 1 in adult monkeys following restricted deafferentation. *Neuroscience*, *8*(1), 33–55. https://doi.org/10.1016/0306-4522(83)90024-6

Merzenich, M. M., Nelson, R. J., Kaas, J. H., Stryker, M. P., Jenkins, W. M., Zook, J. M., Cynader, M. S., & Schoppmann, A. (1987). Variability in hand surface representations in areas 3b and 1 in adult owl and squirrel monkeys [_eprint: https://onlinelibrary.wiley.com/doi/pdf/10.1002/cne.902580208]. *Journal of Comparative Neurology*, *258*(2), 281–296. https://doi.org/10.1002/cne.902580208

Merzenich, M. M., Nelson, R. J., Stryker, M. P., Cynader, M. S., Schoppmann, A., & Zook, J. M. (1984). Somatosensory cortical map changes following digit amputation in adult monkeys [_eprint: https://onlinelibrary.wiley.com/doi/pdf/10.1002/cne.902240 *Journal of Comparative Neurology*, *224*(4), 591–605. https://doi.org/10.1002/cne.902240408

Moreno-Bote, R. (2014). Poisson-like spiking in circuits with probabilistic synapses [Publisher: Public Library of Science]. *PLOS Computational Biology*, *10*(7), e1003522. https://doi.org/10.1371/journal.pcbi.1003522

Mountcastle, V. B., Talbot, W. H., & Kornhuber, H. H. (1966). The neural transformation of mechanical stimuli delivered to the monkey's hand [Section: 19 _eprint: https://onlinelibrary.wiley.com/doi/pdf/10.1002/9780470715338.ch19]. *Ciba foundation symposium - hormonal factors in carbohydrate metabolism (colloquia on endocrinology)* (pp. 325–351). John Wiley & Sons, Ltd. https://doi.org/10.1002/9780470715338.ch19

Nazir, T. A. (1992). Effects of lateral masking and spatial precueing on gap-resolution in central and peripheral vision. *Vision Research*, *32*(4), 771–777. https://doi.org/10.1016/0042-6989(92)90192-L

Nonaka, T., Ito, K., & Stoffregen, T. A. (2021). Structure of variability in scanning movement predicts braille reading performance in children [Number: 1 Publisher: Nature Publishing Group]. *Scientific Reports*, *11*(1), 7182. https://doi.org/10.1038/s41598-021-86674-5

Papadimitriou, V., & Argyropoulos, V. (2017). The effect of hand movements on braille reading accuracy. *International Journal of Educational Research*, *85*, 43–50. https://doi.org/10.1016/j.ijer.2017.07.004

Pei, Y.-C., Denchev, P. V., Hsiao, S. S., Craig, J. C., & Bensmaia, S. J. (2009). Convergence of submodality-specific input onto neurons in primary somatosensory cortex. *Journal of Neurophysiology*, *102*(3), 1843–1853. https://doi.org/10.1152/jn.00235.2009

Pettet, M. W., & Gilbert, C. D. (1992). Dynamic changes in receptive-field size in cat primary visual cortex. *Proceedings of the National Academy of Sciences of the United States of America*, *89*(17), 8366–8370. Retrieved October 22, 2022, from https://www.ncbi.nlm.nih.gov/pmc/articles/PMC49919/

Pruszynski, J. A., & Johansson, R. S. (2014). Edge-orientation processing in first-order tactile neurons [Number: 10 Publisher: Nature Publishing Group]. *Nature Neuroscience*, *17*(10), 1404–1409. https://doi.org/10.1038/nn.3804

Ryles, R. (1996). The impact of braille reading skills on employment, income, education, and reading habits [ERIC Number: EJ526009]. *Journal of Visual Impairment & Blindness*, *90*(3), 219–26.

Schwartz, O., Dayan, P., & Sejnowski, T. J. (2006). A bayesian framework for tilt perception and confidence. *Advances in Neural Information Processing Systems*, *18*. Retrieved November 16, 2021, from https://papers.nips.cc/paper/2005/hash/566a9968b43628588e76be5a85a0f9e8-Abstract.html

Schwartz, O., Hsu, A., & Dayan, P. (2007). Space and time in visual context [Number: 7 Publisher: Nature Publishing Group]. *Nature Reviews Neuroscience*, *8*(7), 522–535. https://doi.org/10.1038/nrn2155

Shadlen, M. N., & Newsome, W. T. (1998). The variable discharge of cortical neurons: Implications for connectivity, computation, and information coding [Publisher: Society for Neuroscience Section: ARTICLE]. *Journal of Neuroscience*, *18*(10), 3870–3896. https://doi.org/10.1523/JNEUROSCI.18-10-03870.1998

Sheffield, R. M., D'Andrea, F. M., Morash, V., & Chatfield, S. (2022). How many braille readers? policy, politics, and perception [Publisher: SAGE Publications

Inc]. *Journal of Visual Impairment & Blindness*, *116*(1), 14–25. https://doi.org/10.1177/0145482X211071125

Shu, Y., Hasenstaub, A., Badoual, M., Bal, T., & McCormick, D. A. (2003). Barrages of synaptic activity control the gain and sensitivity of cortical neurons [Publisher: Society for Neuroscience Section: Cellular/Molecular]. *Journal of Neuroscience*, *23*(32), 10388–10401. https://doi.org/10.1523/JNEUROSCI.23-32-10388.2003

Sripati, A. P., Yoshioka, T., Denchev, P., Hsiao, S. S., & Johnson, K. O. (2006). Spatiotemporal receptive fields of peripheral afferents and cortical area 3b and 1 neurons in the primate somatosensory system. *The Journal of Neuroscience*, *26*(7), 2101–2114. https://doi.org/10.1523/JNEUROSCI.3720-05.2006

Stevens, J. C., & Patterson, M. Q. (1995). Dimensions of spatial acuity in the touch sense: Changes over the life span [Publisher: Taylor & Francis _eprint: https://doi.org/10.3109 *Somatosensory & Motor Research*, *12*(1), 29–47. https://doi.org/10.3109/08990229509063140

Stocker, A. A., & Simoncelli, E. P. (2006). Noise characteristics and prior expectations in human visual speed perception [Bandiera_abtest: a Cg_type: Nature Research Journals Number: 4 Primary_atype: Research Publisher: Nature Publishing Group]. *Nature Neuroscience*, *9*(4), 578–585. https://doi.org/10.1038/nn1669

Sur, M., Merzenich, M. M., & Kaas, J. H. (1980). Magnification, receptive-field area, and "hypercolumn" size in areas 3b and 1 of somatosensory cortex in owl monkeys. [Publisher: American Physiological Society]. *Journal of Neurophysiology*, *44*(2), 295–311. https://doi.org/10.1152/jn.1980.44.2.295

Sur, M., Nelson, R. J., & Kaas, J. H. (1982). Representations of the body surface in cortical areas 3b and 1 of squirrel monkeys: Comparisons with other primates [_eprint: https://onlinelibrary.wiley.com/doi/pdf/10.1002/cne.902110207]. *Journal of Comparative Neurology*, *211*(2), 177–192. https://doi.org/10.1002/cne.902110207

Tomko, G. J., & Crapper, D. R. (1974). Neuronal variability: Non-stationary responses to identical visual stimuli. *Brain Research*, *79*(3), 405–418. https://doi.org/10.1016/0006-8993(74)90438-7

Tong, J., Mao, O., & Goldreich, D. (2013). Two-point orientation discrimination versus the traditional two-point test for tactile spatial acuity assessment. *Frontiers in Human Neuroscience*, *7*. https://doi.org/10.3389/fnhum.2013.00579

Tong, J., Ngo, V., & Goldreich, D. (2016). Tactile length contraction as bayesian inference [Publisher: American Physiological Society]. *Journal of Neurophysiology*, *116*(2), 369–379. https://doi.org/10.1152/jn.00029.2016

Toussaint, K. A., & Tiger, J. H. (2010). TEACHING EARLY BRAILLE LITERACY SKILLS WITHIN a STIMULUS EQUIVALENCE PARADIGM TO CHILDREN WITH DEGENERATIVE VISUAL IMPAIRMENTS. *Journal of Applied Behavior Analysis*, *43*(2), 181–194. https://doi.org/10.1901/jaba.2010.43-181

Turin, G. (1960). An introduction to matched filters [Conference Name: IRE Transactions on Information Theory]. *IRE Transactions on Information Theory*, *6*(3), 311–329. https://doi.org/10.1109/TIT.1960.1057571

Uzuntarla, M., Barreto, E., & Torres, J. J. (2017). Inverse stochastic resonance in networks of spiking neurons [Publisher: Public Library of Science]. *PLOS Computational Biology*, *13*(7), e1005646. https://doi.org/10.1371/journal.pcbi.1005646

Vazquez, Y., Salinas, E., & Romo, R. (2013). Transformation of the neural code for tactile detection from thalamus to cortex. *Proceedings of the National Academy of Sciences*, *110*(28), E2635–E2644. https://doi.org/10.1073/pnas.1309728110

Vega-Bermudez, F., & Johnson, K. O. (1999). Surround suppression in the responses of primate SA1 and RA mechanoreceptive afferents mapped with a probe array [Publisher: American Physiological Society]. *Journal of Neurophysiology*, *81*(6), 2711–2719. https://doi.org/10.1152/jn.1999.81.6.2711

Vega-Bermudez, F., Johnson, K. O., & Hsiao, S. S. (1991). Human tactile pattern recognition: Active versus passive touch, velocity effects, and patterns of confusion [Publisher: American Physiological Society]. *Journal of Neurophysiology*, *65*(3), 531–546. https://doi.org/10.1152/jn.1991.65.3.531

Vega-Bermudez, F., & Johnson, K. O. (2004). Fingertip skin conformance accounts, in part, for differences in tactile spatial acuity in young subjects, but not for the decline in spatial acuity with aging. *Perception & Psychophysics*, *66*(1), 60–67. https://doi.org/10.3758/BF03194861

Warzecha, A.-K., & Egelhaaf, M. (1999). Variability in spike trains during constant and dynamic stimulation [Publisher: American Association for the Advancement of Science]. *Science*, *283*(5409), 1927–1930. https://doi.org/10.1126/science.283.5409.1927

Waschke, L., Kloosterman, N. A., Obleser, J., & Garrett, D. D. (2021). Behavior needs neural variability. *Neuron*, *109*(5), 751–766. https://doi.org/10.1016/j.neuron.2021.01.023

Weber, E. H., Murray, D. J., Ross, H. E., & Weber, E. H. (2018, October 23). *E.h. weber on the tactile senses*. Psychology Press. https://doi.org/10.4324/9781315782089

Weinstein, S. (1968). Intensive and extensive aspects of tactile sensitivity as a function of body part, sex and laterality. *the First Int' l symp. on the Skin Senses, 1968*. Retrieved November 26, 2020, from https://ci.nii.ac.jp/naid/10017541995/en/

Womelsdorf, T., Anton-Erxleben, K., Pieper, F., & Treue, S. (2006). Dynamic shifts of visual receptive fields in cortical area MT by spatial attention [Number: 9 Publisher: Nature Publishing Group]. *Nature Neuroscience*, *9*(9), 1156–1160. https://doi.org/10.1038/nn1748

Xing, J., & Gerstein, G. L. (1996). Networks with lateral connectivity. i. dynamic properties mediated by the balance of intrinsic excitation and inhibition [Publisher: American Physiological Society]. *Journal of Neurophysiology*, *75*(1), 184–199. https://doi.org/10.1152/jn.1996.75.1.184

Yoshioka, T., Dillon, M. R., Beck, G. C., Rapp, B., & Landau, B. (2013). Tactile localization on digits and hand: Structure and development. *Psychological science*, *24*(9), 1653–1663. https://doi.org/10.1177/0956797613478617